Specialization of the Chromatin Remodeler RSC to Mobilize Partially-Unwrapped Nucleosomes

Alisha Schlichter*, Margaret M. Kasten*, Timothy J. Parnell, and Bradley R. Cairns

Howard Hughes Medical Institute (HHMI), Department of Oncological Sciences, Huntsman Cancer Institute, University of Utah School of Medicine, Salt Lake City, Utah, USA.

For correspondence: brad.cairns@hci.utah.edu.

*These authors contributed equally.

Abstract

SWI/SNF-family chromatin remodeling complexes, such as *S. cerevisiae* RSC, slide and eject nucleosomes to regulate transcription. Within nucleosomes, stiff DNA sequences confer spontaneous partial unwrapping, prompting whether and how SWI/SNF-family remodelers are specialized to remodel partially-unwrapped nucleosomes. *RSC1* and *RSC2* are orthologs of mammalian *PBRM1* (polybromo) which define two separate RSC sub-complexes. Remarkably, *in vitro* the Rsc1-containing complex remodels partially-unwrapped nucleosomes much better than does the Rsc2-containing complex. Moreover, a *rsc1*Δ mutation, but not *rsc2*Δ, is lethal with histone mutations that confer partial unwrapping. Rsc1/2 isoforms both cooperate with the DNA-binding proteins Rsc3/30 and the HMG protein, Hmo1, to remodel partially-unwrapped nucleosomes, but show differential reliance on these factors. Notably, genetic impairment of these factors strongly reduces the expression of genes with wide nucleosome-deficient regions (e.g. ribosomal protein genes), known to harbor partially-unwrapped nucleosomes. Taken together, Rsc1/2 isoforms are specialized through composition and interactions to manage and remodel partially-unwrapped nucleosomes.

19 # Introduction

20

21 Nucleosomes regulate transcription in diverse ways and can either block or attract transcriptional
22 regulators (Workman and Kingston 1998, Iyer 2012). At promoters, nucleosome positioning and/or
23 occupancy plays a central role in regulating transcription factor binding, with transitions in nucleosome
24 positioning typically accompanying activation. SWI/SNF-family ATP-dependent chromatin remodeling
25 complexes (CRCs) have evolved to conduct nucleosome sliding and ejection, and enable transcription
26 factor access to DNA. These CRCs are complex in both composition and mechanism; they utilize a
27 catalytic ATPase to translocate DNA around nucleosomes to conduct nucleosome sliding and eviction,
28 and contain an additional set of proteins to help target and regulate each complex (Clapier and Cairns
29 2009, Lorch and Kornberg 2017, Narlikar, Sundaramoorthy, and Owen-Hughes 2013).

30 The SWI/SNF-family remodeler, RSC (Remodels the Structure of Chromatin), from the budding yeast *S.*
31 *cerevisiae,* is both essential and abundant, and has long served as a prototype CRC. RSC complex (like
32 others in the SWI/SNF family) is found in more than one compositional subtype, and contains either
33 Rsc1 or its highly-related paralog, Rsc2 (Cairns et al. 1999). Rsc1 and Rsc2 are orthologs of the
34 mammalian polybromo, as both contain multiple bromodomains, a bromodomain-adjacent homology
35 (BAH) domain, and a DNA binding motif (AT Hook or HMG box). Additional RSC compositional variation
36 has been suggested, involving the association of two additional paralogous RSC subunits, Rsc3 and Rsc30
37 (Campsteijn, Wijnands-Collin, and Logie 2007, Chambers et al. 2012), which are zinc cluster DNA-binding
38 proteins with affinity for GC-rich sequences (Badis et al. 2008). *RSC1* and *RSC2* are redundant for
39 viability (*rsc1*Δ *rsc2*Δ mutants are inviable), however loss of only one confers mild but dissimilar
40 phenotypes, suggesting overlapping essential functions alongside limited unique functions (Baetz et al.
41 2004, Chambers et al. 2012, Cairns et al. 1999, Bungard, Reed, and Winter 2004). To gain further
42 understanding regarding the roles of RSC1 and RSC2 complexes, we characterized Rsc1- and Rsc2-
43 containing complexes through purification and *in vitro* biochemical assays, alongside *in vivo* genetic and
44 genomic characterization. Both approaches converged to reveal an interplay of functional roles for
45 Rsc1/2, Rsc3/30 and a partner high-mobility group (HMG) domain protein, Hmo1, in managing partially-
46 unwrapped nucleosomes.

47 Partially-unwrapped nucleosomes are defined here as those in which the DNA has released (or displays
48 a tendency to release) from the histone octamer at one or both of the symmetric locations where DNA
49 enters/exits the nucleosome, while the central DNA gyre maintains association with the octamer. DNA

50 sequences differ in their affinity for histone octamers and propensity to form nucleosomes (Anderson,
51 Thastrom, and Widom 2002); stiff homopolymer AT tracts deter nucleosome formation (Segal and
52 Widom 2009) whereas those with short (5 bp) alternating AT and GC tracts more easily adopt
53 nucleosomal curvature, providing a lower cost in energy for nucleosome formation. The commonly used
54 '601' nucleosome positioning sequence is synthetic, was selected for high affinity (Lowary and Widom
55 1998), and displays a 5 bp AT/GC alternating pattern. In contrast, the *5S* rRNA gene sequence is
56 naturally occurring, of lesser affinity (comparable to genome averages), and the entry/exit DNA displays
57 higher rates of detachment from the octamer – displaying partial unwrapping (Polach and Widom 1995,
58 Dong, Hansen, and van Holde 1990, Li and Widom 2004, Zhou and Gaullier 2019).

59 Prior work has revealed the presence of partially-unwrapped 'fragile' nucleosomes at promoters with an
60 especially wide nucleosome deficient region (NDR), and co-incidence of RSC, including at the majority of
61 ribosomal protein genes (RPGs) (Kubik et al. 2015, Brahma and Henikoff 2019, Knight et al. 2014).
62 Indeed, *in silico* size fractionation of RSC-bound nucleosomes provides evidence that RSC occupies
63 wrapped nucleosomes at the +1 and -1 promoter positions, as well as a partially-unwrapped
64 nucleosome interposed between those two displaying lower/fractional occupancy – the basis for the
65 appearance of a large NDR (Brahma and Henikoff 2019). As partially-unwrapped nucleosomes are likely
66 conformationally diverse (Bilokapic, Strauss, and Halic 2018), RSC may have evolved to both recognize
67 and remodel these nucleosomes. Prior work with the Rsc2-containing form of RSC revealed altered
68 remodeling outcomes for partially-unwrapped (H3 R40A) nucleosomes (Somers and Owen-Hughes
69 2009), further questioning whether an alternative form of RSC might better manage them. RSC
70 mobilization of partially-unwrapped nucleosomes may allow sets of transcription factors regulated
71 access to a section of DNA without keeping the region constitutively nucleosome-free – which may
72 provide regulatory benefits and help maintain genome stability (see Discussion). Here, we provide
73 multiple lines of evidence that a set of proteins in RSC (Rsc1, Rsc3/30), and interacting with RSC (Hmo1),
74 cooperate to help remodel partially-unwrapped nucleosomes *in vitro* and *in vivo*.

75

76 # Results

77

78 **The Rsc3/30 heterodimer preferentially associates with the RSC1 complex via the CT2 domain**

79 Rsc1 and Rsc2 are highly similar proteins (45% identical, 62% similar), with high homology present in the
80 bromodomains, BAH domain, and the CT1 region – whereas the CT2 region, which is required for Rsc1 or
81 Rsc2 assembly into RSC, is considerably more divergent (Cairns et al. 1999). We began by exploring
82 whether these Rsc1- or Rsc2-containing subtypes differ in composition, beyond Rsc1/2 themselves. To
83 determine, we purified RSC sub-complexes using a TAP tag (Puig et al. 2001) on either Rsc1 or Rsc2,
84 which revealed Rsc3/30 at apparent stoichiometric levels in the Rsc1-containing complex, but
85 substoichiometric levels in the Rsc2-containing complex (**Figure 1A, 1B**) (Chambers et al. 2012).
86 Furthermore, when purifications were conducted under increasing salt conditions, Rsc3/30 association
87 with Rsc1-TAP was maintained, but was lost with Rsc2-TAP (**Figure 1 – figure supplement 1**) confirming
88 higher avidity of Rsc3/30 for the Rsc1 sub-type.

89 To identify whether a particular region within Rsc1 mediates this preferential association with Rsc3/30,
90 we performed domain swaps between Rsc1 and Rsc2 (**Figure 1C**) and checked for complementation and
91 Rsc3 association. To assess this, a *rsc1*Δ *rsc2*Δ strain containing *RSC1* on a *URA3*-marked plasmid was
92 transformed with *TRP1*-marked plasmids containing Rsc1/2 domain swap derivatives, and
93 complementation was demonstrated by their ability to lose the *URA3*-marked *RSC1* plasmid with 5FOA
94 (**Figure 1D).** Here, co-immunoprecipitation revealed strong Rsc3 association with Rsc1, and with Rsc2
95 derivatives only if they contained the CT2 region of Rsc1 (**Figure 1E**). Conversely, strong Rsc3 association
96 with Rsc1 was lost when Rsc1 contained the CT2 region of Rsc2. Similar approaches involving internal
97 Rsc1/2 deletions and additional swap positions provided further refinement, narrowing the region on
98 Rsc1 responsible for strong Rsc3/30 association to residues 617-777 (**Figure 1 – figure supplement 2A-**
99 **D**). Several structures of RSC-nucleosome complexes have recently been published (Wagner et al. 2020,
100 Ye et al. 2019, Patel et al. 2019). However, as Rsc1, Rsc2, Rsc3, and Rsc30 are within the flexible regions,
101 these structures contain only partial models (or lack density/models). While the Rsc1-Rsc3/30
102 interaction has not been resolved structurally, crosslinks were observed between Rsc2 CT2 and Rsc3/30
103 heterodimer (Wagner et al. 2020), an interaction we find to be much stronger in Rsc1.

104

105 **The RSC1 complex slides *5S* nucleosomes better than the RSC2 complex**

106 Having defined and isolated the four main RSC subtypes (RSC1 or RSC2, +/- Rsc3/30; **Figure 2A**), we then
107 tested for differences in ATPase activity, and remodeling efficiency, by examining nucleosomes of typical
108 wrapping/affinity, such as those formed with the sea urchin *5S* DNA nucleosome positioning sequence
109 (NPS) and recombinant yeast histones. First, all four RSC complexes displayed similar DNA-dependent
110 ATPase activities in typical V_{max} determinations with plasmid DNA (**Figure 2B**). The activity of one
111 complex, RSC1-3/30, plateaued earlier than the other RSC complexes, but otherwise the two complexes
112 behaved similarly. However, major differences were observed with *5S* nucleosomes – RSC1 complex
113 displayed much greater sliding activity than RSC2 (**Figure 2C and Figure 2 – figure supplement 1** for
114 quantification). As shown previously for RSC, all sliding activities with RSC1 and RSC2 complexes are ATP
115 dependent ((Cairns et al. 1996) and **Figure 2 – figure supplement 2A**). RSC1 and RSC2 complexes both
116 bound *5S* nucleosomes comparably in the absence of ATP (**Figure 2 – figure supplement 2B**) indicating
117 that their differences in activities occur after the initial engagement of the *5S* nucleosome. Finally, the
118 Rsc3/30 module did not affect their ATPase activities (**Figure 2B**) nor their binding to *5S* nucleosomes
119 (**Figure 2 – figure supplement 2B**); however, in both the RSC1 and RSC2 complexes, Rsc3/30 inclusion
120 moderately inhibited remodeling (**Figure 2C**). Taken together, RSC1 complex displays markedly higher
121 sliding activity on *5S* nucleosomes compared to RSC2 complex.

122 We note that the RSC-remodeled *5S* nucleosomal product migrates more slowly on native gels than the
123 starting nucleosome in our sliding assay. This could result from an altered position of the octamer along
124 the DNA, from the partial unwrapping of DNA from the octamer, or possibly from the creation of a
125 hexasome during the remodeling reaction (which would create a more 'open' and unwrapped
126 structure). To determine whether the slower-migrating RSC remodeled product was the result of
127 H2A/H2B dimer loss from the nucleosome, we assembled 174 bp *5S* nucleosomes using yeast octamers
128 that were fluorescently labeled with Oregon Green (OG) on H2A (Q114C) and conducted sliding assays
129 with RSC1-3/30 (**Figure 2 – figure supplement 3A**). The ratio of H2A to DNA was calculated for both the
130 "start" and "slid" bands at each time point, normalized to the starting nucleosomal band (**Figure 2 –**
131 **figure supplement 3B**). Here, the "slid" band maintained a dimer to DNA ratio similar to the starting
132 nucleosome, rather than that predicted for a hexasome or tetrasome, supporting the identity of the
133 slower-migrating band being an intact nucleosome. We will, therefore, refer to this band on the native
134 gel as the "slid" nucleosome position.

135 ***rsc1*Δ mutation is lethal in combination with histone mutations that confer partial unwrapping**

136 In principle, a variety of factors might underlie better relative remodeling by RSC1 complexes on *5S*
137 nucleosomes. To provide insight into Rsc1/2 differences and to help guide further *in vitro* approaches,
138 we conducted unbiased genetic screens to identify histone mutations that are selectively lethal with
139 *rsc1*Δ or *rsc2*Δ mutations. Here, we utilized an alanine scanning approach in which each of the histone
140 residues is separately mutated to alanine. To implement, we created *rsc1*Δ or *rsc2*Δ deletions
141 (separately) within a 'histone shuffle' strain (*rsc1*Δ or *rsc2*Δ*, h3-h4*Δ [*H3-H4.URA3*]) and combined those
142 with a library encoding all viable histone H3-H4 alanine substitutions on *TRP1*-marked plasmids
143 (Nakanishi et al. 2008). We then assessed viability following enforced loss of the wild-type *H3-H4*
144 plasmid on 5FOA-containing medium. Histone mutations that are lethal with both *rsc1*Δ and *rsc2*Δ, or
145 lethal uniquely with *rsc2*Δ, were found distributed throughout the nucleosome. In striking contrast,
146 those mutations that were lethal specifically with *rsc1*Δ mapped exclusively within the H3 αN helix
147 region – the position where DNA enters/exits the nucleosome (**Table 1, Figure 3A-B**). Furthermore, the
148 specific H3 αN helix mutations obtained in our screen overlap strongly with those reported to increase
149 partial unwrapping using FRET formats (Ferreira et al. 2007), whereas alanine substitutions that did not
150 show a phenotype (P43A, E50A, K56A) had little effect on FRET/unwrapping (**Table 1- table supplement**
151 **1**). Given the results from the H3-H4 screen, we then performed a screen combining *rsc1*Δ or *rsc2*Δ with
152 H2A-H2B mutations (Nakanishi et al. 2008). In keeping with the results above, we find *rsc1*Δ-specific
153 synthetic lethality primarily with mutations in the H2A C-terminus which interact with the H3 αN helix,
154 as well as with specific histone-DNA contacts (H2A R78 and H2A R30; **Figure 3- figure supplement 1).**
155 Taken together, our genetic results, which encompass the entire nucleosome, strongly suggest that
156 synthetic lethality in *rsc1*Δ strains is due to decreased ability of RSC2 complexes to remodel partially-
157 unwrapped nucleosomes relative to RSC1 complexes.

158

159 **Increased Rsc3/30 association with RSC suppresses phenotypes associated with histone αN helix**
160 **mutant combinations**

161 We then explored whether the genetic differences observed with histone αN helix mutations in
162 combination with *rsc1*Δ or *rsc2*Δ involve differential interaction of Rsc1/2 with Rsc3/30. First, we tested
163 whether the CT2 domain of Rsc1, which interacts better with Rsc3/30 than its counterpart in Rsc2, could
164 confer growth when placed within a Rsc2 derivative. Here, growth was clearly restored to *rsc1*Δ H3
165 G44A and *rsc1*Δ H3 R40A combinations with a plasmid encoding Rsc1 or Rsc2 bearing the Rsc1 CT2, but

166 not with Rsc2 or Rsc1 bearing the Rsc2 CT2 (**Figure 3C**). Additional domain swap experiments localize
167 this complementation to the Rsc3/30 association region in Rsc1 (aa 617-777) (**Figure 3 – figure**
168 **supplement 2A**). As a complementary approach, we tested for *RSC3* or *RSC30* high-copy plasmid
169 suppression. While high-copy *RSC3* or *RSC30* could not rescue *rsc1*Δ αN helix histone combined lethality
170 (data not shown), suppression of the strong temperature sensitivity (Ts^-) phenotype of *rsc1*Δ H3 V46A
171 was observed (**Figure 3D**). Taken together, improving the association/functionality of Rsc3/30
172 suppresses phenotypes associated with αN helix histone mutations – further linking Rsc1/2 and Rsc3/30
173 to partial nucleosome unwrapping.

174 **Rsc1/2 differences are largely independent of bromodomain-histone interactions**

175 We then tested the alternative hypothesis that the bromodomains of Rsc1/2 might interact differently
176 with the main acetylated histone residue within/near the αN helix, H3 K56. However, the H3 K56A
177 mutation was not lethal in combination with either *rsc1*Δ or *rsc2*Δ (**Figure 3A**). We then further tested
178 H3 K56Q, which mimics the acetylated form. The K56Q mutation confers synthetic lethality when
179 combined with *rsc1*Δ, but not with *rsc2*Δ (**Figure 3 – figure supplement 2B**). Furthermore, domain
180 swaps involving the highly homologous bromodomains and BAH domains between Rsc1 and Rsc2 did
181 not confer phenotypic differences, nor did these swaps alter the synthetic lethality of *rsc1*Δ with histone
182 αN helix mutations (**Figure 3 – figure supplement 2A**). Notably, H3 K56A has little effect on DNA
183 unwrapping, whereas K56Q promotes unwrapping (Ferreira et al. 2007, Masumoto et al. 2005) – and is
184 lethal with *rsc1*Δ, further supporting an unwrapping function as being responsible for the phenotype.
185 Thus, the lethality with *rsc1*Δ does not appear linked to bromodomains or histone acetylation, in
186 agreement with findings that H3K56 acetylation does not enhance RSC binding (Neumann et al. 2009).

187 **RSC2 complexes are deficient in remodeling partially-unwrapped nucleosomes**

188 Our genetic results prompted the examination of sliding by the RSC1 and RSC2 complexes on *5S*
189 nucleosomes bearing a mutation (e.g., H3 R40A) predicted to confer partial unwrapping. Although
190 sliding of nucleosomes bearing H3 R40A by either form of RSC is reduced relative to wild-type (WT) *5S*
191 nucleosomes, RSC1 complexes were markedly more active than RSC2 complexes (**Figure 3E and Figure 3**
192 **– figure supplement 3** for quantification), reinforcing the difference between RSC1 and RSC2.
193 Additionally, both RSC1 and RSC2 complexes bind H3 αN helix mutant *5S* nucleosomes similarly (**Figure**
194 **3 – figure supplement 4**), demonstrating that initial nucleosome binding is not inhibited by this octamer
195 mutation, suggesting downstream remodeling activity as the affected step. To confirm and better define

196 the extent of partial unwrapping observed on the 174 bp *5S* nucleosome, we conducted ExoIII-S1
197 nuclease mapping (which removes DNA that is either outside of, or not well wrapped in a nucleosome
198 (Flaus 2011), and combined this with a high-throughput paired-end sequencing approach to define the
199 endpoints and proportion of the nuclease-protected species. We found WT 174 bp *5S* yeast
200 nucleosomes display a fully-wrapped side (position 158), and a side of partial unwrapping, in agreement
201 with asymmetric *5S* nucleosome unwrapping previously shown (Winogradoff and Aksimentiev 2019).
202 Here, WT nucleosomes displayed a much higher proportion of largely-wrapped species (≥135 bp) than
203 did H3 R40A nucleosomes **(Figure 3 – figure supplement 5**). Since RSC2 is more deficient than RSC1 in
204 repositioning H3 R40A nucleosomes, the mapping supports the hypothesis that RSC1 complexes manage
205 partially-unwrapped nucleosomes better than RSC2 complexes. We note that H3 R40A *5S* nucleosomes
206 are likely to have a distinct conformation that is not distinguished in our nuclease protection assay, since
207 remodeling by both RSC1 and (more so) by RSC2 complexes is inhibited by the H3 αN helix mutation
208 (compare Figure 3E with Figure 2C). These mutant octamers may enforce a greater degree of openness
209 or distance between the *5S* DNA ends, as demonstrated previously (Ferreira et al. 2007), and thereby
210 inhibit RSC activity (perhaps the transition of binding to DNA translocation, see Discussion) – a
211 nucleosome perturbation better managed by RSC1 complexes.

212 **RSC cooperates with Hmo1 to remodel partially-unwrapped nucleosomes**

213 Hmo1 is an HMGB family protein that stabilizes fragile/partially-unwrapped nucleosomes, particularly at
214 rRNA and ribosomal protein gene promoters (Hall, Wade, and Struhl 2006, Panday and Grove 2017).
215 Unlike other HMGB proteins which have an acidic CTD that promotes bending and nucleosome
216 destabilization, Hmo1 is unique in containing a basic lysine rich C-terminal extension, and has been
217 shown to stabilize chromatin and perform the functions of a linker histone (Panday and Grove 2016).
218 Hmo1 is proposed to bind near the nucleosome dyad and use its basic extension to bind linker DNA and
219 prevent bending (Panday and Grove 2017), which may also improve wrapping and thus cooperate with
220 RSC1 or RSC2 to promote remodeling. We first tested for *rsc/hmo1* genetic interactions by combining
221 *rsc1*Δ or *rsc2*Δ with *hmo1*Δ. Notably, we observe synthetic phenotypes in *rsc1*Δ *hmo1*Δ mutants, but
222 not *rsc2*Δ *hmo1*Δ mutants (**Figure 4A**), suggesting a greater reliance of Rsc2 on Hmo1 for functional
223 cooperativity. Furthermore, as we saw with the H3 αN helix mutations, this synthetic sickness was
224 partially complemented by the presence of the Rsc1 CT2, and partially suppressed by high-copy *RSC3* or
225 *RSC30*, providing further support that these proteins work together in a modular manner (**Figure 4B**).

226 To test RSC-Hmo1 associations *in vivo*, we performed co-immunoprecipitations between Rsc1 and Rsc2
227 with Hmo1. Hmo1 was endogenously tagged at its C-terminus with a V5 epitope in Myc-tagged Rsc1 and
228 Rsc2 strains. Here, crosslinked chromatin extracts were prepared from log phase cells and sonicated, or
229 treated with micrococcal nuclease, resulting primarily in mononucleosomes. Immunoprecipitation
230 with anti-Myc or anti-V5 antibody followed by immunoblot analysis revealed that both Rsc1 and Rsc2
231 co-immunoprecipitate with Hmo1, which represents either a direct interaction between Hmo1 and RSC
232 or colocalization on the same nucleosome(s) (**Figure 4C, Figure 4- figure supplement 1)**. Taken
233 together, Hmo1 shows physical interaction on chromatin with Rsc1 and Rsc2, but strong
234 functional/genetic interaction primarily with Rsc2 (RSC2 complexes are reliant on Hmo1, in a *rsc1*Δ
235 strain).

236 **Hmo1 strongly stimulates the sliding activity of Rsc2, and moderately stimulates Rsc1**

237 Hmo1 stimulates the sliding activity of RSC and SWI/SNF complex *in vitro* on 601 nucleosomes (Hepp et
238 al. 2014), but it is not known whether stimulation applies equally to RSC1 and RSC2 complexes, or has a
239 differential effect on their action upon partially-unwrapped nucleosomes. One explanation for why
240 *rsc1*Δ *hmo1*Δ mutants grow more poorly than *rsc2*Δ *hmo1*Δ mutants is that RSC1 is able to remodel
241 those locations in the absence of Hmo1, but RSC2 is not. As Hmo1 enhances RSC remodeling activity
242 (Hepp et al. 2014), we preincubated the *5S* nucleosomal template with increasing amounts of purified
243 Hmo1 and tested for stimulation of RSC1/2 sliding activity. Interestingly, Hmo1 moderately stimulates
244 RSC1 activity, whereas Hmo1 greatly stimulates RSC2 activity (**Figure 4D and Figure 4 –figure**
245 **supplement 2** for quantification), a property that is even more evident in conditions of limiting
246 remodeler or at early time points (**Figure 4 – figure supplement 3**). Moreover, both RSC1 and RSC2 slide
247 the *5S* nucleosome at lower remodeler concentrations in the presence of Hmo1 (30 nM RSC without
248 Hmo1 compare with 10 nM RSC with Hmo1), further supporting a role for Hmo1 in stimulating RSC
249 remodeling activity.

250 **Well-wrapped nucleosomes are remodeled comparably by both RSC1 and RSC2 complexes**

251 Beyond Hmo1 addition, we explored the ability of RSC1 and RSC2 complexes to remodel nucleosomes
252 bearing a very strong positioning sequence: the optimized 601 sequence. Here, RSC1 and RSC2
253 complexes both displayed robust sliding activity with 601 nucleosomes, with RSC1 activity slightly higher
254 (**Figure 4E and Figure 4 – figure supplement 4** for quantification). We note a correlation here and in
255 prior work (Clapier et al. 2016) between ejection and the use of strong positioning sequences – their

256 initial stability from favored 'phasing' may convert to high instability and disfavored 'phasing' after 5 bp
257 of DNA translocation – which may underlie the progressive ejection observed with 601 nucleosomes.

258 We then explored whether an extremely strong positioning sequence (601) might remain wrapped in
259 the presence of an αN helix mutation and rescue RSC2 remodeling. Indeed, we found robust
260 remodeling of 601 H3 R40A nucleosomes by RSC2 (**Figure 4- figure supplement 5A and Figure 4 – figure**
261 **supplement 6** for quantification**)**, and (by nuclease susceptibility) found that these nucleosomes remain
262 largely wrapped (**Figure 4- figure supplement 5B**). Our data supports the model that while the H3 R40A
263 mutation can result in an open and more loosely wrapped nucleosome conformation, this can be
264 overcome by a strong DNA positioning sequence. In addition, the data indicates that the αN helix H3
265 R40A mutation itself does not impair remodeling by RSC2 unless that mutation confers partial
266 unwrapping due to the underlying DNA sequence.

267 **Rsc1 and Rsc2 both occupy wide NDRs, with Rsc1 specifically occupying tDNAs**

268 RSC has been examined by chromatin co-immunoprecipitation (ChIP) in several formats (Damelin et al.
269 2002, Yen et al. 2012, Vinayachandran et al. 2018, Brahma and Henikoff 2019), though only one study
270 has examined Rsc1/2 differences. This early ChIP approach with microarrays examined Rsc1 and Rsc2
271 differences, and revealed similar promoter targets for RSC1 and RSC2 complexes (Ng et al. 2002).
272 However, possible issues of sensitivity with earlier data combined with the ability to perform more
273 advanced approaches and analyses prompted ChIP-seq experiments to reveal possible differences.
274 Recent examination of Sth1/RSC occupancy by the 'cut and run' MNase approach (which would have
275 superimposed and not distinguished between Rsc1 and Rsc2 occupancy) revealed general enrichment
276 for RSC complexes at many +1 and -1 nucleosomes, as well as high enrichment of RSC within the NDR of
277 genes with very wide NDRs (e.g., ribosomal protein genes). Notably, these wide NDR regions/promoters
278 have been shown to contain RSC bound to partially-unwrapped nucleosomes, rather than the complete
279 lack of nucleosomes (Brahma and Henikoff 2019). Therefore, we will hereafter refer to them as
280 'partially-unwrapped regions' when appropriate, and use the term 'NDR' to generally refer to the
281 nucleosome-deficient regions between the -1 and +1 nucleosome.

282 To further examine the genome-wide location of RSC1 and RSC2 complexes and their relation to
283 nucleosome wrapping, we utilized MYC-tagged derivatives of Rsc1, Rsc2 and Rsc3 (tagged at their
284 endogenous loci) and performed MNase-based ChIP-seq from logarithmically growing cells. We observe
285 RSC at locations similar to prior work (Brahma and Henikoff 2019), and largely comparable profiles

286 between Rsc1 and Rsc2 at most Pol II genes (as described previously (Ng et al. 2002)). However, we
287 observe differential occupancy in two regions: promoters with wide NDRs and tDNAs.

288 First, we observed high occupancy of RSC (Rsc1, Rsc2 and Rsc3; **Figure 5A**) at promoters with wide NDRs,
289 with Rsc1 appearing more enriched than Rsc2. As promoters with partially-unwrapped nucleosomes
290 often contain the HMGB protein, Hmo1, we also compared the occupancy of Hmo1 using the ChIP-seq
291 data (Knight et al, 2014) reprocessed using our parameters. Notably, Hmo1 occupancy positively
292 correlates with regions displaying the widest NDRs and bearing the highest Rsc1 and Rsc2 occupancy,
293 with an apparent higher correlation with Rsc1 (**Figure 5A-D**). The loci with the highest Hmo1 occupancy
294 displayed a mean region size of 336 bp, and a remarkable two-thirds of those genes were ribosomal
295 protein genes (RPGs). Ribosomal protein gene promoters contain GC-rich sequences within their 'NDR'
296 region, and in keeping, we observe Rsc3 enrichment, consistent with Rsc3/30 involvement in targeting
297 or retention.

298 The most striking difference between Rsc1 and Rsc2 occupancy was observed at tDNAs. tDNAs encode
299 tRNAs, and are approximately the size of a single nucleosome - though they are among the most
300 nucleosome-depleted loci in the yeast genome, due at least in part to the action of RSC (Parnell, Huff,
301 and Cairns 2008) and their high fractional occupancy by RNA polymerase III transcription factors (Kumar
302 and Bhargava 2013). Here, Rsc1 complexes are markedly more enriched than Rsc2 complexes, and
303 Hmo1 is notably absent (**Figure 5E, F**). Notably, many tDNAs are flanked by highly AT-rich sequences
304 (Giuliodori et al. 2003), which could (in principle) confer partial unwrapping during the uncommon times
305 (e.g. after replication) when tDNAs are transiently unoccupied by Pol III; here, RSC1 complexes might
306 conduct nucleosome sliding to reveal tDNA sequences to the Pol III machinery. Indeed, the high
307 fractional occupancy of Pol III complexes likely underlies the lack of Hmo1 at tDNAs, as Pol III factors
308 would likely compete with Hmo1 for DNA binding and can remove nucleosomes during transcription.
309 Taken together, Rsc1 and Rsc2 both highly occupy Pol II promoters known to contain partially-
310 unwrapped nucleosomes and Hmo1, whereas Rsc1 preferentially occupies tDNAs.

311 **RSC and HMO1 cooperate to regulate gene expression**

312 To address the transcriptional effects of each of these proteins, we performed RNAseq on
313 logarithmically growing WT, *rsc1*Δ, *rsc2*Δ, *hmo1*Δ, *rsc1*Δ *hmo1*Δ, and *rsc2*Δ *hmo1*Δ cells cultured in SC
314 media. We observe modest differences in transcriptional profiles between WT, *rsc1*Δ, and *rsc2*Δ (**Figure**

315 **5G-H**), which we interpret to be reflective of the known redundancy between Rsc1 and Rsc2 for most
316 functions.

317 However, combining *rsc1*Δ or *rsc2*Δ with *hmo1*Δ resulted in a strong transcriptional shift, resulting in the
318 upregulation (>2-fold) and downregulation (>2-fold) of ~1000 genes (**Figure 5G**), with the most affected
319 class of genes including RPGs, which are downregulated (**Figure 5H**). Additionally the transcriptional shift
320 observed in the double mutants largely mirrors the shift of both up-regulation and down-regulation
321 observed in response to environmental stress response (ESR) genes (Gasch et al. 2000, Brion et al. 2016)
322 (**Figure 5- figure supplement 1).** These results suggest that Rsc1 and Rsc2 both cooperate with Hmo1 to
323 promote the transcription of ribosomal protein genes, and that the burden for chromatin remodeling at
324 these and other growth regulated loci requires the action of both Rsc1 and Rsc2, if Hmo1 is absent.

325 As Rsc3/30 also interacts with and affects Rsc1/2 function, we further analyzed *rsc1*Δ *rsc30*Δ*,* and *rsc2*Δ
326 *rsc30*Δ mutants (**Figure 5- figure supplement 2)**. Remarkably, only *rsc2*Δ *rsc30*Δ mutants strongly impact
327 RP genes – suggesting that the RSC1 complex, which interacts more strongly with Rsc3/30, is more
328 reliant on Rsc3/30 than is the RSC2 complex, and that in a *rsc2*Δ *rsc30*Δ both complexes are impaired
329 (Figure 5- figure supplement 2C).

330 Given our exploration of Rsc1/2 paralog and Rsc3/30 paralog function, we also explored their evolution.
331 A whole genome duplication (WGD) occurred within the *Saccharomyces* lineage approximately 150
332 million years ago (Wolfe and Shields 1997) resulting in *RSC1/2* paralogs. We find the single *RSC1/2*
333 ortholog present in species that did not undergo the WGD (e.g. *Zygosaccharomyces, Ashbya*, and
334 *Lachancea*), more closely related to *RSC2* than *RSC1*, suggesting *RSC2* as the more ancient ortholog
335 (**Figure 5- figure supplement 3)**. Notably, species more distant to *S. cerevisiae* lack both *RSC3* and
336 *RSC30*. Following the appearance of *RSC3*, the WGD event then created *RSC1/2* and *RSC3/RSC30*
337 orthologs, along with duplications of the ribosomal protein genes, a large fraction of which have been
338 maintained in *Saccharomyces cerevisiae*. Finally, *HMO1* predates the appearance of *RSC3* and the WGD
339 and is found in *Schizosaccharomyces pombe* (Albert et al. 2013). Thus, specialization of Rsc1 to
340 preferentially bind Rsc3/30 and play a role in the regulation of the ribosomal protein genes was enabled
341 by the WGD, and may have arisen to help rapidly and properly regulate RPGs in response to growth
342 conditions.

343 Taken together, our results are consistent with RSC1 complexes bearing a higher intrinsic ability to
344 mobilize partially-unwrapped nucleosomes compared to RSC2, augmented by partner proteins that

345 preferentially assist either RSC1 (Rsc3/30) or RSC2 (Hmo1) complexes to more efficiently remodel at
346 locations with partially-wrapped nucleosomes (**Figure 6**).

347

348 # DISCUSSION

349

350 Genomes are diverse in DNA sequence composition, and the biophysical properties of DNA – in
351 particular, DNA curvature and stiffness – creating a spectrum of affinities for nucleosomes, the main
352 packaging unit of chromatin. This spectrum can undergo selection to create regions where nucleosome
353 formation, positioning, and/or turnover is favored or disfavored, properties which can be utilized at
354 promoters and enhancers to help regulate transcription factor binding, transcription, and ultimately
355 fitness. These biophysical properties work in concert (and sometimes in opposition) with the action of
356 chromatin remodelers, which utilize ATP to move nucleosomes to either favored or disfavored positions,
357 and to eject nucleosomes to provide regulated access of transcription factors to DNA. The commonness
358 in yeast of stiff/disfavored DNA sequences at proximal promoters, juxtaposed to bendable/favorable
359 sequences at the -1 and +1 positions (especially at constitutive or highly transcribed genes), raises the
360 possibility that chromatin remodelers may have undergone specialization to manage the remodeling of
361 both fully wrapped and partially-unwrapped nucleosomes.

362 Here, we provide several lines of evidence that the RSC1 complex can slide partially-unwrapped
363 nucleosomes better than its paralog, the RSC2 complex. Furthermore, as RSC is assisted by additional
364 proteins (e.g. Hmo1) that augment this function *in vivo* , RSC can be thought of as two functional
365 entities: 'Rsc2 with Hmo1' and 'Rsc1 with Rsc3-30', with strong phenotypes only observed when both
366 entities are impaired (**Figure 6**). First, we find that RSC1 acts more efficiently on *5S* nucleosomes, and
367 retains activity on nucleosomes bearing H3 R40A, a mutation that favors unwrapping, whereas RSC2 is
368 relatively impaired. Second, an unbiased genetic screen revealed synthetic lethality with *rsc1*Δ αN helix
369 combinations, but not *rsc2*Δ αN helix combinations, strongly suggesting that the RSC2 complex has
370 more difficulty remodeling partially-unwrapped nucleosomes. Third, Hmo1 stabilizes nucleosomes
371 (Panday and Grove 2016, 2017), and we observe synthetic phenotypes with *rsc1*Δ *hmo1*Δ mutants, but
372 not with *rsc2*Δ *hmo1*Δ mutants (**Figure 4A**), suggesting that Rsc2 relies much more on Hmo1 for
373 functional cooperativity than does Rsc1. This result is paralleled in our remodeling experiments, which
374 show a more pronounced rescue of *5S* nucleosome sliding by RSC2 complexes than RSC1 complexes

375 with recombinant Hmo1 (**Figure 4D**). We note that as nucleosome binding affinity is very similar
376 between RSC1 and RSC2 complexes, the defect/challenge in remodeling with the RSC2 complex may
377 involve a step downstream of binding, perhaps involving the ability of the complex to commit to the
378 initiation of DNA translocation, which may be sensitive to the conformation of the nucleosome.
379 Alternatively, nucleosome conformation/wrapping may impact the efficiency of DNA translocation –
380 termed 'coupling' – which involves the probability of each ATP hydrolysis resulting in 1 bp of productive
381 DNA translocation, a property known to be regulated in RSC complex by the actin-related proteins, Arp7
382 and Arp9 (Clapier et al. 2016, Szerlong et al. 2008). Finally, we emphasize that partially-unwrapped
383 nucleosomes are not preferred by RSC1 complex over wrapped nucleosomes; RSC1 simply manages
384 partially-unwrapped nucleosomes better than does RSC2 complex.

385 Initially, it may seem counter-intuitive for partial unwrapping of a nucleosome to impede rather than
386 enhance RSC remodeling. However, we note that partial unwrapping is not an intermediate to full
387 unwrapping – as full unwrapping followed by full octamer re-wrapping is not the mechanism of
388 nucleosome sliding. Therefore, a partially-unwrapped nucleosome is not necessarily a remodeling
389 intermediate, and therefore not necessarily stimulatory. Instead, we suggest that sliding involves a 1-
390 bp/ATP DNA translocation mechanism imposed on a fully wrapped, or partially-wrapped nucleosome.
391 Here, we suggest that partial unwrapping results in a nucleosome conformation that can indeed be
392 encountered/bound by RSC1/2 complexes, but resists transition to the DNA translocation phase of
393 remodeling – with RSC2 complexes less able to conduct this transition than RSC1 complexes (**Figure 6**). A
394 second related model would be that RSC1 complex might better induce or stabilize a wrapped
395 nucleosome conformation that is more conducive to initiating or continuing remodeling.

396 Above, we show that the product of remodeling (using *5S* nucleosomes formed with yeast octamers)
397 migrates more slowly than does the initial substrate, and (by using Oregon Green-labeled H2A) that the
398 product is not a hexasome or tetrasome involving H2A-H2B dimer loss. Nucleosome migration is
399 determined by both the octamer position along the DNA (center vs end-positioned), and the overall
400 shape of the octamer-DNA complex, including the extent to which the product/slid nucleosome is
401 wrapped – as partial unwrapping and an 'open' conformation would be predicted to result in a slower
402 migrating species through a native gel, just as a more 'compact' conformation results in a faster
403 migrating species (Chakravarthy, Patel, and Bowman 2012).

404 The mammalian polybromo protein (PBRM1) helps define the PBAF sub-complex of mammalian
405 SWI/SNF complex, and is similar in domain composition to the combination of Rsc1/2 and the Rsc4

406 protein (which contains multiple bromodomains). PBRM1 also contains an HMG domain, which is
407 notably absent in the Rsc1, 2, and 4 combination of domains. Here, we speculate that the Hmo1 protein
408 and the HMG domain of PBRM1 may have functional similarities in managing DNA wrapping, which can
409 be tested in future work.

410 RSC contains two proteins with affinity for GC-rich sequences: the paralogs Rsc3 and Rsc30. Here, we
411 reveal a higher avidity of the Rsc3/30 module for the RSC1 complex, localize the region of interaction of
412 Rsc3/30 with Rsc1/2 to the beginning of the CT2 domain, and provide genetic evidence that the
413 preferred interaction of Rsc3/30 with Rsc1 has functional consequences. A current curiosity is the
414 observation – true for both Rsc1 and Rsc2 complexes – that the presence of Rsc3/30 moderately inhibits
415 remodeling, while the genetics supports a positive role for Rsc3/30 in assisting Rsc1/2 function. One
416 obvious role for Rsc3/30 is in targeting RSC to GC-rich promoter sequences such as ribosomal protein
417 genes, which likely underlies the essential nature of Rsc3/30 function. Here, future work may explore
418 whether Rsc3/30 serve a regulatory role in the remodeling reaction, with their modest attenuation
419 function relieved in the proper regulatory contexts of DNA sequence (e.g., GC richness) and protein
420 composition (e.g., Hmo1, others) to help confer environmental sensing and properly regulate RPGs.

421 In favorable growth conditions, approximately 50% of the transcriptional effort of RNA Pol II is directed
422 at RPGs (Warner 1999). Our work supports and greatly extends the prior work of others (Knight et al.
423 2014, Hepp et al. 2017, Wade, Hall, and Struhl 2004) that *S. cerevisiae* has evolved many ways to 'poise'
424 chromatin at RPG promoters in a relatively 'open and ready' format. These promoters have evolved to
425 be less favorable to nucleosomes by bearing regions of 'stiff' AT-rich DNA (Segal and Widom 2009)
426 (note: Rsc1/2 each bear an AT hook), are punctuated by GC-rich DNA (known Rsc3/30 binding sites), and
427 use histone acetylation (e.g. H3 K56ac) (Neumann et al. 2009), Hmo1 (Hall, Wade, and K. Struhl, 2006),
428 DNA-binding general regulatory factors (e.g. Rap1, Abf1) and chromatin remodeling complexes such as
429 RSC and SWI/SNF complex – that together help keep these regions nucleosome deficient and partially-
430 unwrapped (Kubik et al. 2018, Hepp et al. 2017, Brahma and Henikoff 2019, Reja et al. 2015). While
431 RSC1 and RSC2 complexes appear largely redundant at most genes, and can both be assisted at RPG
432 promoters by Hmo1, our work supports the notion that the RSC1 complex, through its ability to better
433 manage partially-unwrapped nucleosomes and preferential association with Rsc3/30, has become
434 specialized to help perform this role (**Figure 6**). This combination of specialization and partial
435 redundancy provides this system the needed robustness and the ability to conduct rapid and

436 sophisticated activation/regulation of this important RPG class – attributes which may contribute to
437 fitness in diverse environments.

438

439 # MATERIALS AND METHODS

440

441 **Strains, Media, Yeast growth, and Assay Replication**

442 Rich media (YPD), synthetic complete (SC), and sporulation media were prepared using standard
443 methods. Standard procedures were used for transformations, sporulation, tetrad analysis and spotting.
444 A null mutation of Hmo1 was obtained from Invitrogen and crossed into *rsc1* and *rsc2* deletion strains.
445 Rsc1 was C-terminally TAP-tagged as described by (Rigaut et al. 1999), and Hmo1 C-terminally tagged
446 with V5 as described in (Funakoshi and Hochstrasser 2009). Full genotypes of yeast strains are available
447 in **Supplementary File 1**. A technical replicate is defined as a test of the same sample multiple times,
448 whereas a biological replicate is defined as the same test run on multiple biological samples of
449 independent origin. The number and type of replicates for each experiment is indicated in the figure
450 legend.

451 **Plasmid Construction**

452 DNA encoding Rsc1 w/Rsc2 CT2 was created by PCR amplification of RSC2 CT2 from position K617
453 through the end of the gene, using primers containing 40bp homology to *RSC1* or vector sequence. PCR
454 product was co-transformed with linearized p609 (314.RSC1) into YBC800 (rsc1Δ rsc2Δ [316.RSC1]) and
455 homologous recombination inserted the DNA encoding CT2 into *RSC1* beginning at position K617. Rsc2
456 w/1CT2 at position K656 was created by amplifying *RSC1* CT2 on p609 (314.RSC1) and co-transforming
457 into linearized p604 (314.RSC2) into YBC803 (*rsc1Δ rsc2Δ* [316.RSC2]) and repaired by homologous
458 recombination. Plasmid was isolated from TRP positive colonies, sequenced, and retransformed to check
459 for complementation. Additional swaps were constructed similarly. Internal deletions in Rsc1 and Rsc2
460 were created by digesting with restriction enzymes with blunt or compatible ends, removing the small
461 fragment and ligating ends back together. Plasmid markers were swapped as needed as described in
462 (Cross 1997). A full list of plasmids used in this study is provided in **Supplementary File 2**.

463 **RSC1 and RSC2 TAP purification**

464 RSC complexes were purified from *S. cerevisiae* strains BCY211 (RSC2-TAP) and BCY516 (RSC1-TAP)
465 harboring an integrated version of the C-terminally Tandem Affinity Purification (TAP)-tagged on the
466 construct of the indicated gene. Purifications were performed essentially as described (Rigaut et al.
467 1999) (Szerlong et al. 2008) with the following modifications. After harvesting, cells were washed with

468 0.5x PBS + 10% glycerol, pelleted, and frozen in liquid nitrogen as pea-size pieces. Frozen cells were
469 pulverized in a SPEX SamplePrep 6850 Freezer/Mill at a rate of 10, for 10 cycles of 3 min 'on' and 2 min
470 'off', with the resulting powder stored at -80°C until purification.

471 RSC1+3/30 complex was purified from BCY516 essentially as described (Szerlong et al. 2008) with the
472 following modifications since Rsc1 is found at lower levels than Rsc2 in yeast cells. Pulverized cells (160
473 g) were solubilized in Lysis Buffer (50 mM HEPES [pH 7.5], 400 mM KOAc, 10 mM EDTA, 20% glycerol, 0.5
474 mM BME, protease inhibitors). The KOAc concentration of the lysate was brought to 450 mM and
475 nucleic acids were precipitated with 0.1-0.2% polyethyleneimine. The cleared lysate was incubated with
476 5 ml IgG Sepharose 6 Fast Flow (GE Healthcare) for 3 h, the resin sequentially washed with Lysis Buffer,
477 IgG Wash Buffer (20 mM Tris-Cl, [pH 8], 400 mM KOAc, 0.1% Igepal, 1 mM EDTA, 0.5 mM BME, protease
478 inhibitors), and IgG Elution Buffer (20 mM Tris-Cl [pH 8], 200 mM KOAc, 10% glycerol, 0.1% Igepal, 0.5
479 mM BME). The RSC1-TAP complex was cleaved from the IgG resin with 500 U AcTEV enzyme (Invitrogen)
480 gently rotating the slurry at 15°C for 1 h followed by 4°C rotation overnight. The eluate was collected,
481 brought to 3 mM $CaCl_2$, and bound to 1.5 ml Calmodulin Affinity Resin (Agilent Technologies) overnight.
482 The resin was washed with 250 Calmodulin Wash Buffer (20 mM Tris-Cl [pH 7.5], 250 mM NaCl, 1 mM
483 Mg Acetate, 1 mM imidazole, 2 mM CaCl2, 10% glycerol, 0.1% Igepal, 0.5 mM BME, protease inhibitors).
484 The RSC1 complex was eluted with 250 Calmodulin Elution Buffer (20 mM Tris-Cl [pH 7.5], 250 mM NaCl,
485 2 mM EGTA, 10% glycerol, 0.1% Igepal, 0.5 mM BME, protease inhibitors) in successive 500-750 µl
486 fractions. The RSC1-containing fractions were determined, pooled, and residual nucleic acid was
487 removed by a final DEAE Sepharose clean-up step. The complex was concentrated on a Vivaspin 30K PES
488 concentrator, concentration was determined by Bradford assay (Bio-Rad) and confirmed by silver
489 stained polyacrylamide SDS-PAGE analysis.

490 RSC1-3/30 complex was purified as described above except the IgG Wash Buffer had 750 mM NaCl
491 instead of KOAc, and the IgG resin was rotated overnight during the IgG Wash step to remove the
492 Rsc3/30 module. The bound IgG resin was equilibrated into IgG Elution Buffer before cleaving with
493 AcTEV.

494 RSC2+3/30 complex was purified as above with the following modifications. Approximately 80 g of
495 pulverized BCY211 cells were solubilized in Lysis Buffer. Cleared lysates were incubated with IgG
496 Sepharose, washed and eluted with AcTEV enzyme as above. The eluate was collected, brought to 3 mM
497 $CaCl_2$, and bound to 1.5 ml Calmodulin Affinity Resin for 3 h. The resin was washed with 200 KOAc
498 Calmodulin Wash (same as Calmodulin Wash but with 200 mM KOAc replacing the NaCl) followed by

499 150 NaCl Calmodulin Wash (same as Calmodulin Wash but with 150 mM NaCl). The RSC2 complex was
500 eluted with 150 Calmodulin Elution Buffer (same as above but with 150 mM NaCl) in successive 500-750
501 μl fractions. The RSC2-containing fractions were determined and pooled. The salt was increased to 250
502 mM NaCl and residual nucleic acid was removed on DEAE Sepharose. The complex was immediately
503 diluted to 125 mM NaCl while maintaining the other buffer component concentrations. The complex
504 was concentrated and the concentration was determined as above.

505 RSC2-3/30 complex was purified essentially as the RSC2+3/30 complex with the following modifications.
506 After binding the Calmodulin Affinity Resin, the resin was washed with 200 KOAc Calmodulin Wash
507 Buffer, followed by four 20 min washes with 500 mM NaCl Calmodulin Wash Buffer, and a final rinse
508 with 150 NaCl Calmodulin Wash Buffer to equilibrate the resin. The RSC2-3/30 complex was eluted from
509 the Calmodulin Affinity Resin, residual nucleic acid removed on DEAE Sepharose, concentrated and
510 quantified as above for the RSC2+3/30 complex.

511 **Hmo1 Purification**

512 Recombinant Hmo1 was purified from bacteria as an N-terminal fusion to 8xHIS (plasmid from T.
513 Formosa). Briefly, *E. coli* BL21-CodonPlus(DE3)RIL transformed with pET.8xHIS.Hmo1 was induced with
514 IPTG at 30°C for 3 h to express the fusion protein. Cells were harvested, resuspended in HIS Lysis Buffer
515 (20 mM Tris [pH 8], 500 mM NaCl, 10 mM imidazole, 10% glycerol, 0.1% Igepal, 1.5 mM BME, protease
516 inhibitors), and lysed by sonication. The lysate was cleared and bound to pre-equilibrated Ni-NTA
517 agarose beads (Qiagen) for 1.5 h. The bound resin was washed sequentially with HIS tag Lysis Buffer, Ni
518 Wash Buffer A (same as HIS Lysis Buffer but with 30 mM imidazole), and Ni Wash Buffer B (same as HIS
519 Lysis Buffer but with 50 mM imidazole). The protein was eluted with Ni Elution Buffer (20 mM Tris [pH
520 8], 500 mM NaCl, 250 mM imidazole, 10% glycerol, 0.005% Igepal, 1.5 mM BME, protease inhibitors) and
521 sized on a Superdex 200 gel filtration column (GE). Hmo1 ran as a soluble aggregate (approximately 440
522 kD) larger than predicted from its molecular weight (27.5 kD). The Hmo1 protein was dialyzed into 150
523 mM Sizing Buffer (20 mM Tris [pH 8], 150 mM NaCl, 10% glycerol, 1.5 mM BME, protease inhibitors) and
524 concentrated before storing at -80°C in aliquots.

525 **RSC1 and RSC2 Rsc3/30 Stringency Testing**

526 Stringency testing on Rsc3/30 association with RSC1 and RSC2 was conducted on IgG Sepharose. Cells
527 were grown and pulverized as for RSC purification. Sixty grams of RSC1-TAP cells and 20 g of RSC2-TAP
528 cells were solubilized in Lysis Buffer and the lysate was cleared as above. One milliliter of IgG resin was

529 incubated with the cleared lysate for 2 h. The beads were washed with Lysis Buffer, and then with IgG
530 Wash Buffer, before being split into 10 separate Eppendorf tubes for testing. The beads were gently
531 pelleted, rinsed 3 times with the specific IgG Wash Buffer containing 150, 250, or 500 mM NaCl, as
532 indicated. The specific IgG Wash Buffer was added for 1 h or 16 h (overnight), as indicated. All beads
533 were washed 3 times with IgG Elution Buffer, resuspended in IgG Elution Buffer, and RSC was released
534 from the beads with AcTEV enzyme as above and 1/10th of the eluate was analyzed by silver stain on a
535 6% SDS polyacrylamide gel.

536 **Co-Immunoprecipitations**

537 Whole cell extracts were prepared and co-immunoprecipitations for RSC were performed as described,
538 (Cairns et al. 1999) with the following modification. Anti-Myc or anti-HA antibodies (0.6 µg) were bound
539 to a 25 µl slurry of pan-mouse magnetic Dynabeads (Thermo Fisher) and incubated with 1000 µg of
540 extract. Blots were probed with anti-Sth1 (Saha, Wittmeyer, and Cairns 2002), anti-Rsc3, anti-Rsc30
541 (Angus-Hill et al. 2001), anti-Rsc2 and anti-Rsc4 (Kasten et al. 2004).

542 Extracts for Rsc1 and Rsc2 chromatin co-IPs with Hmo1 were prepared from cells grown to OD_{600}= 0.8,
543 Cultures were crosslinked in 1% formaldehyde final for 30min at RT, quenched with 0.2M glycine, and
544 lysed by bead-beating (mini-beadbeater, Biospec) in LB140 buffer. Samples were sonicated in a
545 Bioruptor Pico (Diagenode) to release chromatin or MNase treated with 100U of micrococcal nuclease
546 for 15 minutes at 37◦C. Immunoprecipitations were performed with 1000 µg of extract and a 25 µl slurry
547 of pan-mouse Dynabeads bound to anti-Myc (Abcam) or anti-V5 (Thermo-Fisher) antibodies.

548 **Nucleosome Assembly**

549 Yeast octamers were produced using purified *S. cerevisiae* histones expressed in *E. coli* BL21-
550 CodonPlus(DE3)RIL. Either wild-type histone H3 or the H3 R40A mutant was assembled into yeast
551 octamers by salt-dialysis, essentially as described previously (Dyer et al. 2004). Mononucleosomes were
552 assembled from a linear salt gradient dialysis (2 M to 50 mM KCl) using Slide-A-Lyser Mini Dialysis units
553 with a 7,000 molecular weight cutoff (Thermo Scientific) essentially as described (Clapier et al. 2016)
554 using one of several DNA positioning sequences. The 205 bp Widom 601 positioning sequence (Lowary
555 and Widom 1998) were produced from pUC12x601 digested with AvaI and purified using preparative
556 electrophoresis (PrepCell, Bio-Rad). The 174 bp sea urchin *5S* positioning sequence was prepared by PCR
557 amplification using a plasmid containing a copy of the sea urchin *5S* sequence as a template. The PCR
558 product was precipitated before purifying on a PrepCell. The exact 601 and *5S* positioning sequences

559 used are given in **File Supplement 2**. Assembled mononucleosomes were separated from free DNA by
560 gradient sedimentation on a 10-30% sucrose gradient as previously described (Wittmeyer, Saha, and
561 Cairns 2004). Yeast octamers bearing H2A fluorescently labeled with Oregon Green on Q114C were a gift
562 from L. McCullough and T. Formosa. These labeled yeast octamers were assembled into nucleosomes
563 with the 174 bp 5S NPS and purified as described above.

564 **ATPase Assays**

565 Measurement of ATP hydrolysis was as described previously (Saha, Wittmeyer, and Cairns 2002,
566 Wittmeyer, Saha, and Cairns 2004) using a color (malachite green) absorbance assay that quantitatively
567 measures released free phosphate. Time courses were performed on two separate purifications of each
568 type of RSC complex. Reactions were performed in triplicate. Activities were measured at V_{max} using
569 double-stranded Bluescript plasmid as the substrate.

570 **Nucleosome Sliding Assay**

571 Nucleosome sliding assays were performed as described (Clapier et al. 2016) with the following
572 modifications. Reactions were conducted in 10 mM Tris [pH 7.4], 50 mM KCl, 3 mM $MgCl_2$, 0.1 mg/ml
573 BSA, 1 mM ATP with 20 nM mononucleosomes at 30°C and 400 rpm shaking in a Thermomixer
574 (Eppendorf). The amount of remodeler varied. Sliding reactions on 205 bp 601 nucleosomes used 10 nM
575 RSC. Sliding reactions on 174 bp *5S* nucleosomes used 30 nM RSC unless otherwise indicated. Aliquots
576 were removed at each time point and reactions were stopped by adding 10 mM EDTA + 200 ng
577 competitor DNA (Bluescript plasmid). Samples were loaded with 10% glycerol on a 4.5% (37.5:1) native
578 polyacrylamide gel and run in 0.4x TBE for 45 min at 110 V constant. Gels were stained with ethidium
579 bromide solution and scanned on a Typhoon Trio (Amersham, GE).

580 **Nucleosome Gel Shift Assays**

581 Nucleosome gel shift assays were conducted similarly to the nucleosome sliding assay described above
582 with the following modifications. Reactions were conducted in the absence of ATP and at 30°C for 20
583 min with 20 nM mononucleosomes. The RSC remodelers were added at 30 and 60 nM. The reactions
584 were loaded on to 3.8% (37.5:1) native polyacrylamide gels and run in 0.4x TBE for 55 min at 110 V
585 constant without addition of any stop solution or competitor. Gels were stained with ethidium bromide
586 solution and scanned on a Typhoon Trio.

587 **Histone Mutant Screen**

588 Null mutations in *rsc1* and r*sc2* were crossed into the H3/H4 shuffle strain WZY42 (Zhang et al. 1998).
589 Strains YBC1939 (WZY42), YBC2090 and YBC3040 and YBC3221 and YBC3547 were transformed in 96
590 well plate format with a TRP-marked histone H3-H4 or H2A-H2B mutant plasmid library respectively,
591 obtained from and screened as described previously (Nakanishi et al. 2008). Transformants were
592 spotted to SC-TRP plates, replica plated again to SC-TRP plates after 2 days, followed by replica plating
593 to SC-TRP and SC-TRP + 5FOA. Synthetic lethality with mutations in the H3 αN helix were confirmed by a
594 second round of individual transformations and shuffles.

595 **Recombinant Nucleosome Mapping**

596 The position and wrapping of the recombinant nucleosomes were determined by sequencing the
597 protected DNA fragment after treating assembled nucleosomes with Exonuclease III and S1 nuclease.
598 Approximately 400-800 fmol of nucleosomes purified from sucrose gradients was digested with a 5-25U
599 titration of ExoIII enzyme (New England Biolabs) for 1, 2, or 3 min at 37°C in ExoIII Buffer (10 mM Tris
600 [pH 8], 50 mM NaCl, 3 mM $MgCl_2$). Reactions were moved to ice, S1 Buffer and NaCl were added (30 mM
601 NaOAc [pH 4.6], 1 mM ZnOAc, 5% glycerol, and 300 mM NaCl final concentration), and treated with 50U
602 S1 for 30 min at room temperature. Tris [pH 8.8] and EDTA were added to final concentrations of 88 mM
603 and 14 mM, respectively, and heated to 70°C for 10 min. SDS was added to 1%, vortexed, and iced. The
604 protected DNA fragments were cleaned up on a Qiagen MinElute PCR purification column and eluted in
605 30 μl EB. The level of digestion was determined for each sample on a 4.5% (37.5:1) native
606 polyacrylamide 0.4x TBE gel as described above.

607 Libraries were made from the above protected fragments using the NEBNext ChIP-Seq MasterMix Set
608 (New England Biolabs) with the following modifications. Samples did not go through the initial End-
609 Repair. A custom adaptor with an 8 bp unique molecular identifier (UMI) was ligated onto the dA-tailed
610 samples. The UMI Adaptor was created from an oligo based on the standard NEBNext adaptor sequence
611 incorporating 8 random nucleotides at the 5' end of the oligo (see oligo sequence in **File Supplement 2**).
612 To create the UMI Adaptor, 25 μM oligo (synthesized by IDT) was first heated to 95°C and slow cooled
613 to room temperature in Duplex Buffer (100 mM KOAc, 30 mM HEPES [pH 7.5]). The ends of the
614 annealed UMI Adaptor were filled in using Klenow (New England Biolabs). The reaction was stopped
615 with EDTA and heat. The adaptor was cleaned up on a Micro Bio-Spin 6 chromatography column (Bio-
616 Rad) equilibrated with water. A dT-tail was added to the adaptor with Klenow exo- (New England
617 Biolabs). The UMI Adaptor was cleaned up on a Micro Bio-Spin 6 column and eluted in water. The UMI
618 Adaptor was diluted to 1.14 μM final concentration for use in library preparations. High-throughput

619 sequencing was performed by Illumina's protocol for 50 bp paired-end runs on an Illumina HiSeq 2500
620 or a MiSeq.

621 The embedded UMI code was first extracted from the Fastq files using the script
622 embedded_UMI_extractor from the package UMIScripts
623 (https://github.com/HuntsmanCancerInstitute/UMIScripts). Output Fastq sequences were then aligned
624 to an index comprised of the recombinant sea urchin *5S* or 601 sequence using Novocraft Novoalign
625 (version 3.8.2), giving the adapter sequences for trimming. After alignment, PCR-duplicate reads were
626 identified and marked based on the UMI information with the UMISripts application bam_umi_dedup.
627 The 5' start positions for each alignment, discarding duplicates, were recorded as a bigWig file with 1 bp
628 resolution using the application bam2wig from the BioToolBox package
629 (https://github.com/tjparnell/biotoolbox). Separate bigWig files were generated for each length of
630 alignments (92-169 bp). To normalize for sequencing read depth, alignment counts were scaled to an
631 equivalent of 100K reads (calculated from the total sum of alignments without regard to alignment
632 length). Count matrices for each length at each position on the reference sequence and for each sample
633 were then collected using the BioToolBox application get_datasets from the bigWig files. Count matrices
634 were analyzed with Microsoft Excel employing a 5% cutoff of the normalized fragment count.

635 **ChIP Seq and Analysis**

636 Yeast cultures from yHN1 (YBC1544-RSC1.9XMYC) and yHN2 (YBC1545; RSC2.9XMYC) (Ng et al. 2002)
637 were grown in SC-TRP at 30°C with two biological replicates. Cultures were harvested at OD_{600}= 0.8, and
638 crosslinked with 1% formaldehyde final for 30 min at room temperature. Cultures were quenched with
639 0.2M glycine for 5 min. Chromatin extracts were prepared by bead-beating, and chromatin was
640 liberated with micrococcal nuclease. Immunoprecipitation was performed using anti-cMyc 9E11
641 (Abcam). DNA was isolated for input and IP samples and assembled into a library using Illumina
642 protocols and sequenced as single end reads on an Illumina sequencer.

643 Fastq sequences were aligned to the yeast genome (UCSC version SacCer3) with NovoCraft Novoalign
644 (version 3.8.2), allowing for one random alignment for multi-mapping reads. To maintain processing
645 consistency between single-end and paired-end alignments, paired-end was aligned as single-end by
646 ignoring the second read. Alignments were processed using the MultiRepMacsChIPSeq pipeline (version
647 10.1, https://github.com/HuntsmanCancerInstitute/MultiRepMacsChIPSeq). Since MNase-digested
648 chromatin yields high levels of coordinate-duplicate alignments (observed mean of 65%, range 57% to

649 74%), duplicate alignments were randomly subsampled to a uniform rate of 40% to remove sample bias
650 while retaining relative signal intensity. Alignments over ribosomal DNA, telomeric sequences,
651 mitochondrial chromosome, and other high copy sequences were excluded. Fragment coverage tracks
652 were generated by extending alignments in the 3' direction by 160 bp in all fragments. We note that
653 there may be some between-sample biases in the distribution of MNase-digested fragment lengths,
654 particularly with RSC-enriched fragments, but rationalized that uniformity of processing should help
655 minimize these biases. Replicates were depth-normalized (Reads Per Million) prior to combining as an
656 average after confirming reasonable similarity to each through standard correlation metrics. Log2 fold
657 enrichment of ChIP signal over non-enriched nucleosome signal (Input) was generated with Macs2
658 (Zhang et al. 2008) without background lambda correction. Hmo1 ChIPs (GSM1509041) (Knight et al.
659 2014) were re-processed in a similar manner.

660 NDRs were determined by first determining all nucleosome positions in the genome using the software
661 package biotoolbox-nucleosome (https://github.com/tjparnell/biotoolbox-nucleosome) with the Input
662 MNase sample alignments. To reduce mapping noise and increase efficacy of calling positions, "skinny"
663 nucleosome coverage was used rather than midpoint data. Fragment coverage was generated by
664 shifting the 5' alignment coordinate in the 3' direction by 37 bp and extending 74 bp, essentially
665 recording the predicted central portion of the nucleosome. After mapping nucleosomes, NDRs were
666 extracted by calculating all inter-nucleosomal intervals and selecting for those with lengths between 75
667 and 600 bp and occurring over or adjacent to a defined protein-coding gene TSS. NDRs were sorted by
668 decreasing length and aligned by the edge closest to the TSS; NDRs between divergent promoter pairs
669 are represented once.

670 Data was collected with applications from the BioToolBox package
671 (https://github.com/tjparnell/biotoolbox). Mean occupancy of RSC and Hmo1 were collected over the
672 NDRs using the application get_datasets, while spatial data surrounding NDRs and tDNAs were collected
673 with get_relative_data. Heat maps were generated in R (R Core Team 2018) with pHeatmap (Kolde
674 2019). Dot plots and violin plots were generated with GraphPad Prism.

675 **RNA seq and Analysis**

676 Yeast cultures for RNASeq were grown in SD media supplemented for auxotrophic amino acids at 30°C in
677 three biological replicates. RNA from logarithmically growing cells was purified using Ambion Ribo-pure
678 yeast kit. Samples were additionally DNAse-treated and cleaned up with Qiagen RNeasy kit. Illumina

679 Ribo Zero yeast kit was used for library preparation, and sequencing performed on an Illumina
680 sequencer.

681 Fastq reads were processed following an RNASeq pipeline
682 (https://github.com/HuntsmanCancerInstitute/hciR). Briefly, reads were aligned with STAR (version
683 2.5.4, (Dobin et al. 2013), counts obtained with Subread featureCounts (version 1.6.3) based on Ensembl
684 annotation (release 90), and differential gene expression performed with DESeq2 (version 1.21). Dot
685 plots and violin plots were generated with GraphPad Prism (version 8.0.2).

686 **Acknowledgements:**

We thank Brian Dalley and the High-Throughput Sequencing Shared Resource for sequencing data. We thank Ali Shilatifard, Tim Formosa, Jef Boeke, Kevin Struhl, Anne Grove, Roger Kornberg and Sharon Dent for strains, plasmids, and labeled yeast octamer. We thank Patrick Murphy and Edward Grow for helpful discussions on data analysis and experimental design and Naveen Verma, Tim Formosa, and Mahesh Chandrasekharan for feedback on the manuscript. We thank HHMI for support of A.S, M.K and B.C, and thank NCI CA042014 to Huntsman Cancer Institute for support of core facilities. A.S., M.K., and B.C. designed the project. A.S. and M.K. conducted the experiments and prepared the figures. T.P. provided genomics analysis and genomics figures. B.C. wrote the manuscript with contributions from all authors.

Competing Interests

None of the authors have competing financial or non-financial interests related to the work in this manuscript.

687 **Supplemental Information**

688 Figure 1- figure supplement 1. The Rsc3/30 module associates with the Rsc1 complex at high stringency.
689 Figure 1- figure supplement 2. Additional swaps and truncations define the region of Rsc3/30
690 association.
691 Figure 2- figure supplement 1. Quantification of RSC sliding 174 bp 5S wild-type yeast mononucleosomes
692 as conducted in Figure 2C.
693 Figure 2 – figure supplement 2. RSC complexes without Rsc3/30 module are ATP-dependent chromatin
694 remodelers and RSC1 and RSC2 complexes bind similarly to 174b bp sea urchin *5S* mononucleosomes.

695 Figure 2 – figure supplement 3. The RSC *5S* sliding product is not the result of H2A/H2B dimer loss.
696 Table Supplement 1. DNA end to end FRET measurement on mononucleosomes containing H3 αN helix
697 mutations with the phenotype when combined with *rsc1*Δ, *rsc2*Δ.
698 Figure 3- figure supplement 1. Synthetic lethal mutations in each of the four histones H2A, H2B, H3 and
699 H4 when combined with *rsc1*Δ or *rsc2*Δ mutations.
700 Figure 3- figure supplement 2. Complementation by CT2 domain swaps when combined with H3 αN
701 helix mutations.
702 Figure 3- figure supplement 3. Quantification of RSC sliding 174 bp *5S* H3 R40A yeast mononucleosomes
703 as conducted in Figure 3E.
704 Figure 3 – figure supplement 4. RSC1 and RSC2 complexes bind similarly to 174 bp sea urchin *5S* yeast
705 mononucleosomes with the H3 R40A mutation.
706 Figure 3 – figure supplement 5. Mapping the positions of the wt and H3 R40A 174 bp sea urchin *5S* yeast
707 mononucleosomes.
708 Figure 4 – figure supplement 1. Co-Immunoprecipitation of Rsc1 and Rsc2 with Hmo1 from MNase-
709 treated chromatin extracts.
710 Figure 4- figure supplement 2. Quantification of Hmo1 stimulation of RSC sliding 174 bp 5S wild-type
711 yeast mononucleosomes as conducted in Figure 4D.
712 Figure 4 – figure supplement 3. Additional sliding assays and quantification of 174bp *5S* yeast
713 mononucleosomes pre-incubated with increasing concentrations of Hmo1.
714 Figure 4 – figure supplement 4. Quantification of RSC sliding 205 bp Widom 601 wild-type yeast
715 mononucleosomes as conducted in Figure 4E.
716 Figure 4- figure supplement 5. RSC1 and RSC2 complexes slide Widom 601 H3 R40A mononucleosomes
717 similarly.
718 Figure 4 – figure supplement 6. Quantification of RSC sliding 205 bp Widom 601 H3 R40A yeast
719 mononucleosomes as conducted in Figure 4 – figure supplement 5A.
720 Figure 5- figure supplement 1. Gene expression changes in *rsc1*Δ, *rsc2*Δ, and *hmo1*Δ mutants.
721 Figure 5- figure supplement 2. Gene expression changes in *rsc1*Δ, *rsc2*Δ, and *rsc30*Δ mutants.
722 Figure 5- figure supplement 3. Appearance of *RSC1/RSC2*, *RSC3/RSC30* and *HMO1* orthologs in yeast
723 evolution.
724 Supplementary File 1. Table of yeast strains and their genotypes used in this study.
725 Supplementary File 2. Table of plasmids and DNA sequences used in this study.
726 Figure 3- figure supplement 5- Source data 1. 174bp *5S* nucleosome mapping.

727 Figure 4- figure supplement 5B- Source data 1. 205 bp Widom 601 nucleosome mapping.

728 Figure 5- Source data 1- Files for generation of occupancy heat maps.

729 Figure 5- Source data 2- RSC occupancy at promoters and tDNAs.

730 Figure 5- Source data 3- Differential gene expression.

731 Figure 5- figure supplement 1- Source data 1- List of ESR affected genes.

732

733 Raw sequencing data is available at NCBI under SRA accession number PRJNA573112.

734

735 References

736

737 Albert, B., C. Colleran, I. Leger-Silvestre, A. B. Berger, C. Dez, C. Normand, J. Perez-Fernandez, B. McStay,
738 and O. Gadal. 2013. "Structure-function analysis of Hmo1 unveils an ancestral organization of
739 HMG-Box factors involved in ribosomal DNA transcription from yeast to human." *Nucleic Acids*
740 *Res* 41 (22):10135-49. doi: 10.1093/nar/gkt770.
741 Anderson, J. D., A. Thastrom, and J. Widom. 2002. "Spontaneous access of proteins to buried
742 nucleosomal DNA target sites occurs via a mechanism that is distinct from nucleosome
743 translocation." *Molecular and Cellular Biology* 22 (20):7147-7157. doi:
744 10.1128/Mcb.22.20.7147-7157.2002.
745 Angus-Hill, M. L., A. Schlichter, D. Roberts, H. Erdjument-Bromage, P. Tempst, and B. R. Cairns. 2001. "A
746 Rsc3/Rsc30 zinc cluster dimer reveals novel roles for the chromatin remodeler RSC in gene
747 expression and cell cycle control." *Mol Cell* 7 (4):741-51. doi: 10.1016/S1097-2765(01)00219-2.
748 Badis, G., E. T. Chan, H. van Bakel, L. Pena-Castillo, D. Tillo, K. Tsui, C. D. Carlson, A. J. Gossett, M. J.
749 Hasinoff, C. L. Warren, M. Gebbia, S. Talukder, A. Yang, S. Mnaimneh, D. Terterov, D. Coburn, A.
750 Li Yeo, Z. X. Yeo, N. D. Clarke, J. D. Lieb, A. Z. Ansari, C. Nislow, and T. R. Hughes. 2008. "A library
751 of yeast transcription factor motifs reveals a widespread function for Rsc3 in targeting
752 nucleosome exclusion at promoters." *Mol Cell* 32 (6):878-87. doi:
753 10.1016/j.molcel.2008.11.020.
754 Baetz, K. K., N. J. Krogan, A. Emili, J. Greenblatt, and P. Hieter. 2004. "The ctf13-30/CTF13 genomic
755 haploinsufficiency modifier screen identifies the yeast chromatin remodeling complex RSC,
756 which is required for the establishment of sister chromatid cohesion." *Mol Cell Biol* 24 (3):1232-
757 44. doi: 10.1128/mcb.24.3.1232-1244.2003.
758 Bilokapic, S., M. Strauss, and M. Halic. 2018. "Histone octamer rearranges to adapt to DNA unwrapping."
759 *Nat Struct Mol Biol* 25 (1):101-108. doi: 10.1038/s41594-017-0005-5.
760 Brahma, S., and S. Henikoff. 2019. "RSC-Associated Subnucleosomes Define MNase-Sensitive Promoters
761 in Yeast." *Mol Cell* 73 (2):238-249.e3. doi: 10.1016/j.molcel.2018.10.046.
762 Brion, C., D. Pflieger, S. Souali-Crespo, A. Friedrich, and J. Schacherer. 2016. "Differences in
763 environmental stress response among yeasts is consistent with species-specific lifestyles." *Mol*
764 *Biol Cell* 27 (10):1694-705. doi: 10.1091/mbc.E15-12-0816.
765 Bungard, D., M. Reed, and E. Winter. 2004. "RSC1 and RSC2 are required for expression of mid-late
766 sporulation-specific genes in Saccharomyces cerevisiae." *Eukaryot Cell* 3 (4):910-8. doi:
767 10.1128/ec.3.4.910-918.2004.

768 Cairns, B. R., Y. Lorch, Y. Li, M. Zhang, L. Lacomis, H. Erdjument-Bromage, P. Tempst, J. Du, B. Laurent,
769 and R. D. Kornberg. 1996. "RSC, an essential, abundant chromatin-remodeling complex." *Cell* 87
770 (7):1249-60. doi: 10.1016/s0092-8674(00)81820-6.
771 Cairns, B. R., A. Schlichter, H. Erdjument-Bromage, P. Tempst, R. D. Kornberg, and F. Winston. 1999.
772 "Two functionally distinct forms of the RSC nucleosome-remodeling complex, containing
773 essential AT hook, BAH, and bromodomains." *Molecular Cell* 4 (5):715-723. doi: Doi
774 10.1016/S1097-2765(00)80382-2.
775 Campsteijn, C., A. M. Wijnands-Collin, and C. Logie. 2007. "Reverse genetic analysis of the yeast RSC
776 chromatin remodeler reveals a role for RSC3 and SNF5 homolog 1 in ploidy maintenance." *PLoS*
777 *Genet* 3 (6):e92. doi: 10.1371/journal.pgen.0030092.
778 Chakravarthy, S., A. Patel, and G. D. Bowman. 2012. "The basic linker of macroH2A stabilizes DNA at the
779 entry/exit site of the nucleosome." *Nucleic Acids Res* 40 (17):8285-95. doi: 10.1093/nar/gks645.
780 Chambers, A. L., P. M. Brownlee, S. C. Durley, T. Beacham, N. A. Kent, and J. A. Downs. 2012. "The two
781 different isoforms of the RSC chromatin remodeling complex play distinct roles in DNA damage
782 responses." *PLoS One* 7 (2):e32016. doi: 10.1371/journal.pone.0032016.
783 Clapier, C. R., and B. R. Cairns. 2009. "The biology of chromatin remodeling complexes." *Annu Rev*
784 *Biochem* 78:273-304. doi: 10.1146/annurev.biochem.77.062706.153223.
785 Clapier, C. R., M. M. Kasten, T. J. Parnell, R. Viswanathan, H. Szerlong, G. Sirinakis, Y. Zhang, and B. R.
786 Cairns. 2016. "Regulation of DNA Translocation Efficiency within the Chromatin Remodeler
787 RSC/Sth1 Potentiates Nucleosome Sliding and Ejection." *Mol Cell* 62 (3):453-461. doi:
788 10.1016/j.molcel.2016.03.032.
789 Cross, F. R. 1997. "'Marker swap' plasmids: convenient tools for budding yeast molecular genetics."
790 *Yeast* 13 (7):647-53. doi: 10.1002/(SICI)1097-0061(19970615)13:7<647::AID-YEA115>3.0.CO;2-#.
791 Damelin, M., I. Simon, T. I. Moy, B. Wilson, S. Komili, P. Tempst, F. P. Roth, R. A. Young, B. R. Cairns, and
792 P. A. Silver. 2002. "The genome-wide localization of Rsc9, a component of the RSC chromatin-
793 remodeling complex, changes in response to stress." *Mol Cell* 9 (3):563-73. doi: 10.1016/S1097-
794 2765(02)00475-6.
795 Dobin, A., C. A. Davis, F. Schlesinger, J. Drenkow, C. Zaleski, S. Jha, P. Batut, M. Chaisson, and T. R.
796 Gingeras. 2013. "STAR: ultrafast universal RNA-seq aligner." *Bioinformatics* 29 (1):15-21. doi:
797 10.1093/bioinformatics/bts635.
798 Dong, F., J. C. Hansen, and K. E. van Holde. 1990. "DNA and protein determinants of nucleosome
799 positioning on sea urchin 5S rRNA gene sequences in vitro." *Proc Natl Acad Sci U S A* 87
800 (15):5724-8. doi: 10.1073/pnas.87.15.5724.
801 Dyer, P. N., R. S. Edayathumangalam, C. L. White, Y. Bao, S. Chakravarthy, U. M. Muthurajan, and K.
802 Luger. 2004. "Reconstitution of nucleosome core particles from recombinant histones and
803 DNA." *Methods Enzymol* 375:23-44. doi: 10.1016/s0076-6879(03)75002-2.
804 Ferreira, H., J. Somers, R. Webster, A. Flaus, and T. Owen-Hughes. 2007. "Histone tails and the H3
805 alphaN helix regulate nucleosome mobility and stability." *Mol Cell Biol* 27 (11):4037-48. doi:
806 10.1128/mcb.02229-06.
807 Flaus, Andrew. 2011. "Principles and practice of nucleosome positioning in vitro." *Frontiers in Life*
808 *Science* 5 (1-2):5-27. doi: 10.1080/21553769.2012.702667.
809 Funakoshi, M., and M. Hochstrasser. 2009. "Small epitope-linker modules for PCR-based C-terminal
810 tagging in Saccharomyces cerevisiae." *Yeast* 26 (3):185-92. doi: 10.1002/yea.1658.
811 Gasch, A. P., P. T. Spellman, C. M. Kao, O. Carmel-Harel, M. B. Eisen, G. Storz, D. Botstein, and P. O.
812 Brown. 2000. "Genomic expression programs in the response of yeast cells to environmental
813 changes." *Mol Biol Cell* 11 (12):4241-57. doi: 10.1091/mbc.11.12.4241.

814 Giuliodori, S., R. Percudani, P. Braglia, R. Ferrari, E. Guffanti, S. Ottonello, and G. Dieci. 2003. "A
815 composite upstream sequence motif potentiates tRNA gene transcription in yeast." *J Mol Biol*
816 333 (1):1-20. doi: 10.1016/j.jmb.2003.08.016.
817 Hall, D. B., J. T. Wade, and K. Struhl. 2006. "An HMG protein, Hmo1, associates with promoters of many
818 ribosomal protein genes and throughout the rRNA gene locus in Saccharomyces cerevisiae."
819 *Mol Cell Biol* 26 (9):3672-9. doi: 10.1128/mcb.26.9.3672-3679.2006.
820 Hepp, M. I., V. Alarcon, A. Dutta, J. L. Workman, and J. L. Gutierrez. 2014. "Nucleosome remodeling by
821 the SWI/SNF complex is enhanced by yeast high mobility group box (HMGB) proteins." *Biochim*
822 *Biophys Acta* 1839 (9):764-72. doi: 10.1016/j.bbagrm.2014.06.014.
823 Hepp, M. I., M. Smolle, C. Gidi, R. Amigo, N. Valenzuela, A. Arriagada, A. Maureira, M. M. Gogol, M.
824 Torrejon, J. L. Workman, and J. L. Gutierrez. 2017. "Role of Nhp6 and Hmo1 in SWI/SNF
825 occupancy and nucleosome landscape at gene regulatory regions." *Biochim Biophys Acta Gene*
826 *Regul Mech* 1860 (3):316-326. doi: 10.1016/j.bbagrm.2017.01.002.
827 Hyland, Edel M., Michael S. Cosgrove, Henrik Molina, Dongxia Wang, Akhilesh Pandey, Robert J. Cottee,
828 and Jef D. Boeke. 2005. "Insights into the role of histone H3 and histone H4 core modifiable
829 residues in Saccharomyces cerevisiae." *Molecular and cellular biology* 25 (22):10060-10070. doi:
830 10.1128/MCB.25.22.10060-10070.2005.
831 Iyer, V. R. 2012. "Nucleosome positioning: bringing order to the eukaryotic genome." *Trends Cell Biol* 22
832 (5):250-6. doi: 10.1016/j.tcb.2012.02.004.
833 Kasten, M., H. Szerlong, H. Erdjument-Bromage, P. Tempst, M. Werner, and B. R. Cairns. 2004. "Tandem
834 bromodomains in the chromatin remodeler RSC recognize acetylated histone H3 Lys14." *Embo j*
835 23 (6):1348-59. doi: 10.1038/sj.emboj.7600143.
836 Knight, B., S. Kubik, B. Ghosh, M. J. Bruzzone, M. Geertz, V. Martin, N. Denervaud, P. Jacquet, B. Ozkan, J.
837 Rougemont, S. J. Maerkl, F. Naef, and D. Shore. 2014. "Two distinct promoter architectures
838 centered on dynamic nucleosomes control ribosomal protein gene transcription." *Genes Dev* 28
839 (15):1695-709. doi: 10.1101/gad.244434.114.
840 Kolde, Raivo. 2019. "Pretty Heatmaps. Available online at https://cran.r-
841 project.org/web/packages/pheatmap/pheatmap.pdf."
842 Kubik, S., M. J. Bruzzone, P. Jacquet, J. L. Falcone, J. Rougemont, and D. Shore. 2015. "Nucleosome
843 Stability Distinguishes Two Different Promoter Types at All Protein-Coding Genes in Yeast." *Mol*
844 *Cell* 60 (3):422-34. doi: 10.1016/j.molcel.2015.10.002.
845 Kubik, S., E. O'Duibhir, W. J. de Jonge, S. Mattarocci, B. Albert, J. L. Falcone, M. J. Bruzzone, F. C. P.
846 Holstege, and D. Shore. 2018. "Sequence-Directed Action of RSC Remodeler and General
847 Regulatory Factors Modulates +1 Nucleosome Position to Facilitate Transcription." *Mol Cell* 71
848 (1):89-102.e5. doi: 10.1016/j.molcel.2018.05.030.
849 Kumar, Y., and P. Bhargava. 2013. "A unique nucleosome arrangement, maintained actively by
850 chromatin remodelers facilitates transcription of yeast tRNA genes." *BMC Genomics* 14:402.
851 doi: 10.1186/1471-2164-14-402.
852 Li, G., and J. Widom. 2004. "Nucleosomes facilitate their own invasion." *Nat Struct Mol Biol* 11 (8):763-
853 9. doi: 10.1038/nsmb801.
854 Lorch, Y., and R. D. Kornberg. 2017. "Chromatin-remodeling for transcription." *Q Rev Biophys* 50:e5. doi:
855 10.1017/s003358351700004x.
856 Lowary, P. T., and J. Widom. 1998. "New DNA sequence rules for high affinity binding to histone octamer
857 and sequence-directed nucleosome positioning." *J Mol Biol* 276 (1):19-42. doi:
858 10.1006/jmbi.1997.1494.
859 Masumoto, H., D. Hawke, R. Kobayashi, and A. Verreault. 2005. "A role for cell-cycle-regulated histone
860 H3 lysine 56 acetylation in the DNA damage response." *Nature* 436 (7048):294-8. doi:
861 10.1038/nature03714.

862 Nakanishi, S., B. W. Sanderson, K. M. Delventhal, W. D. Bradford, K. Staehling-Hampton, and A.
863 Shilatifard. 2008. "A comprehensive library of histone mutants identifies nucleosomal residues
864 required for H3K4 methylation." *Nat Struct Mol Biol* 15 (8):881-8. doi: 10.1038/nsmb.1454.
865 Narlikar, G. J., R. Sundaramoorthy, and T. Owen-Hughes. 2013. "Mechanisms and functions of ATP-
866 dependent chromatin-remodeling enzymes." *Cell* 154 (3):490-503. doi:
867 10.1016/j.cell.2013.07.011.
868 Neumann, H., S. M. Hancock, R. Buning, A. Routh, L. Chapman, J. Somers, T. Owen-Hughes, J. van Noort,
869 D. Rhodes, and J. W. Chin. 2009. "A method for genetically installing site-specific acetylation in
870 recombinant histones defines the effects of H3 K56 acetylation." *Mol Cell* 36 (1):153-63. doi:
871 10.1016/j.molcel.2009.07.027.
872 Ng, H. H., F. Robert, R. A. Young, and K. Struhl. 2002. "Genome-wide location and regulated recruitment
873 of the RSC nucleosome-remodeling complex." *Genes Dev* 16 (7):806-19. doi:
874 10.1101/gad.978902.
875 OhÉigeartaigh, Seán, David Armisén, Kevin Byrne, and Kenneth Wolfe. 2011. "Systematic discovery of
876 unannotated genes in 11 yeast species using a database of orthologous genomic segments."
877 *BMC genomics* 12:377. doi: 10.1186/1471-2164-12-377.
878 Panday, A., and A. Grove. 2016. "The high mobility group protein HMO1 functions as a linker histone in
879 yeast." *Epigenetics Chromatin* 9:13. doi: 10.1186/s13072-016-0062-8.
880 Panday, A., and A. Grove. 2017. "Yeast HMO1: Linker Histone Reinvented." *Microbiol Mol Biol Rev* 81
881 (1). doi: 10.1128/mmbr.00037-16.
882 Parnell, T. J., J. T. Huff, and B. R. Cairns. 2008. "RSC regulates nucleosome positioning at Pol II genes and
883 density at Pol III genes." *Embo j* 27 (1):100-10. doi: 10.1038/sj.emboj.7601946.
884 Patel, A. B., C. M. Moore, B. J. Greber, J. Luo, S. A. Zukin, J. Ranish, and E. Nogales. 2019. "Architecture of
885 the chromatin remodeler RSC and insights into its nucleosome engagement." *Elife* 8. doi:
886 10.7554/eLife.54449.
887 Polach, K. J., and J. Widom. 1995. "Mechanism of protein access to specific DNA sequences in chromatin:
888 a dynamic equilibrium model for gene regulation." *J Mol Biol* 254 (2):130-49. doi:
889 10.1006/jmbi.1995.0606.
890 Puig, O., F. Caspary, G. Rigaut, B. Rutz, E. Bouveret, E. Bragado-Nilsson, M. Wilm, and B. Seraphin. 2001.
891 "The tandem affinity purification (TAP) method: a general procedure of protein complex
892 purification." *Methods* 24 (3):218-29. doi: 10.1006/meth.2001.1183.
893 R Core Team. 2018. "R: A language and environment for statistical computing." R Foundation for
894 Statistical Computing. Available online at https://www.R-project.org/.
895 Reja, R., V. Vinayachandran, S. Ghosh, and B. F. Pugh. 2015. "Molecular mechanisms of ribosomal
896 protein gene coregulation." *Genes Dev* 29 (18):1942-54. doi: 10.1101/gad.268896.115.
897 Rigaut, G., A. Shevchenko, B. Rutz, M. Wilm, M. Mann, and B. Seraphin. 1999. "A generic protein
898 purification method for protein complex characterization and proteome exploration." *Nat*
899 *Biotechnol* 17 (10):1030-2. doi: 10.1038/13732.
900 Saha, A., J. Wittmeyer, and B. R. Cairns. 2002. "Chromatin remodeling by RSC involves ATP-dependent
901 DNA translocation." *Genes Dev* 16 (16):2120-34. doi: 10.1101/gad.995002.
902 Segal, E., and J. Widom. 2009. "Poly(dA:dT) tracts: major determinants of nucleosome organization."
903 *Curr Opin Struct Biol* 19 (1):65-71. doi: 10.1016/j.sbi.2009.01.004.
904 Somers, J., and T. Owen-Hughes. 2009. "Mutations to the histone H3 alpha N region selectively alter the
905 outcome of ATP-dependent nucleosome-remodelling reactions." *Nucleic Acids Res* 37 (8):2504-
906 13. doi: 10.1093/nar/gkp114.
907 Szerlong, H., K. Hinata, R. Viswanathan, H. Erdjument-Bromage, P. Tempst, and B. R. Cairns. 2008. "The
908 HSA domain binds nuclear actin-related proteins to regulate chromatin-remodeling ATPases."
909 *Nat Struct Mol Biol* 15 (5):469-76. doi: 10.1038/nsmb.1403.

910 Vinayachandran, Vinesh, Rohit Reja, Matthew J. Rossi, Bongsoo Park, Lila Rieber, Chitvan Mittal, Shaun
911 Mahony, and B. Franklin Pugh. 2018. "Widespread and precise reprogramming of yeast protein-
912 genome interactions in response to heat shock." *Genome research* 28 (3):357-366. doi:
913 10.1101/gr.226761.117.
914 Wade, J. T., D. B. Hall, and K. Struhl. 2004. "The transcription factor Ifh1 is a key regulator of yeast
915 ribosomal protein genes." *Nature* 432 (7020):1054-8. doi: 10.1038/nature03175.
916 Wagner, F. R., C. Dienemann, H. Wang, A. Stutzer, D. Tegunov, H. Urlaub, and P. Cramer. 2020.
917 "Structure of SWI/SNF chromatin remodeller RSC bound to a nucleosome." *Nature* 579
918 (7799):448-451. doi: 10.1038/s41586-020-2088-0.
919 Warner, J. R. 1999. "The economics of ribosome biosynthesis in yeast." *Trends Biochem Sci* 24 (11):437-
920 40. doi: 10.1016/s0968-0004(99)01460-7.
921 Winogradoff, D., and A. Aksimentiev. 2019. "Molecular Mechanism of Spontaneous Nucleosome
922 Unraveling." *J Mol Biol* 431 (2):323-335. doi: 10.1016/j.jmb.2018.11.013.
923 Wittmeyer, J., A. Saha, and B. Cairns. 2004. "DNA translocation and nucleosome remodeling assays by
924 the RSC chromatin remodeling complex." *Methods Enzymol* 377:322-43. doi: 10.1016/S0076-
925 6879(03)77020-7.
926 Wolfe, K. H., and D. C. Shields. 1997. "Molecular evidence for an ancient duplication of the entire yeast
927 genome." *Nature* 387 (6634):708-13. doi: 10.1038/42711.
928 Workman, J. L., and R. E. Kingston. 1998. "Alteration of nucleosome structure as a mechanism of
929 transcriptional regulation." *Annu Rev Biochem* 67:545-79. doi:
930 10.1146/annurev.biochem.67.1.545.
931 Ye, Y., H. Wu, K. Chen, C. R. Clapier, N. Verma, W. Zhang, H. Deng, B. R. Cairns, N. Gao, and Z. Chen.
932 2019. "Structure of the RSC complex bound to the nucleosome." *Science* 366 (6467):838-843.
933 doi: 10.1126/science.aay0033.
934 Yen, K., V. Vinayachandran, K. Batta, R. T. Koerber, and B. F. Pugh. 2012. "Genome-wide nucleosome
935 specificity and directionality of chromatin remodelers." *Cell* 149 (7):1461-73. doi:
936 10.1016/j.cell.2012.04.036.
937 Zhang, W., J. R. Bone, D. G. Edmondson, B. M. Turner, and S. Y. Roth. 1998. "Essential and redundant
938 functions of histone acetylation revealed by mutation of target lysines and loss of the Gcn5p
939 acetyltransferase." *EMBO J* 17 (11):3155-67. doi: 10.1093/emboj/17.11.3155.
940 Zhang, Y., T. Liu, C. A. Meyer, J. Eeckhoute, D. S. Johnson, B. E. Bernstein, C. Nusbaum, R. M. Myers, M.
941 Brown, W. Li, and X. S. Liu. 2008. "Model-based analysis of ChIP-Seq (MACS)." *Genome Biol* 9
942 (9):R137. doi: 10.1186/gb-2008-9-9-r137.
943 Zhou, K., and G. Gaullier. 2019. "Nucleosome structure and dynamics are coming of age." 26 (1):3-13.
944 doi: 10.1038/s41594-018-0166-x.

945

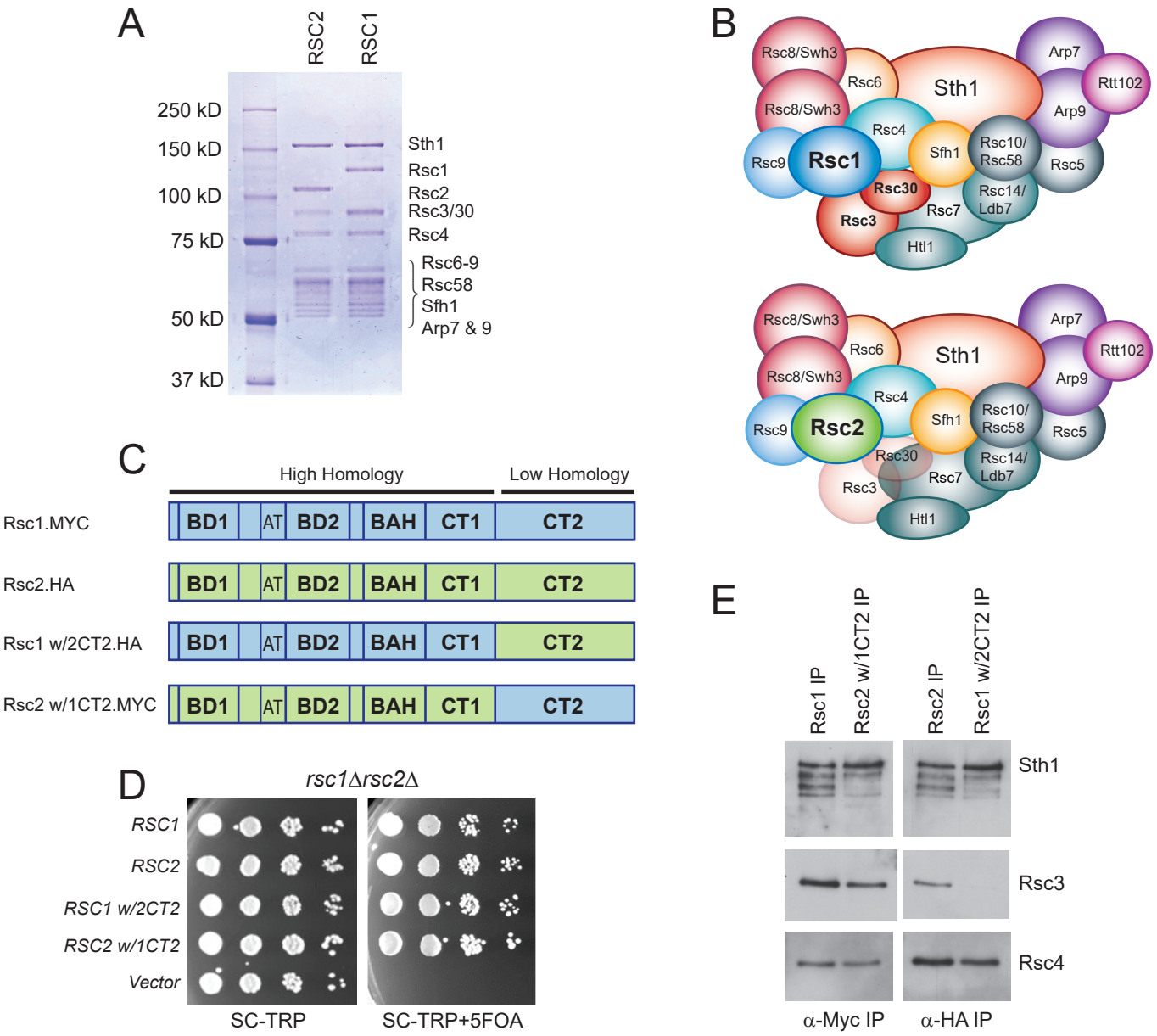

Figure 1. Rsc3/30 module has higher avidity for the RSC1 complex. (A) Purified RSC1-TAP and RSC2-TAP complexes (2 μg) analyzed on 7.5% SDS-PAGE gel stained with Coomassie dye. (B) RSC1 and RSC2 complex compositions, with decreased opacity displaying the reduced association of the Rsc3/30 module in the RSC2 complex. (C) Domain structure and swaps of Rsc1 and Rsc2. (D) CT2 domain swaps complement for viability. *TRP1*-marked plasmids bearing *RSC1* (p609), *RSC2* (p604), *RSC1 w/2CT2* (p3097), *RSC2 w/1CT2* (p3098), or vector (pRS314) were transformed into *rsc1Δrsc2Δ* [*RSC1.URA3*] (YBC800), and spotted as 10x serial dilutions to SC-TRP or to SC-TRP+5FOA to force the loss of the *RSC1.URA3* plasmid. 'w/' indicates 'with'. One of four biological replicates shown. (E) The Rsc3/30 module associates more strongly with the CT2 region of Rsc1. Immunoprecipitations of Rsc1, Rsc2 w/1CT2, Rsc2, Rsc1 w/2CT2 from whole cell extracts. Blots were probed with anti-Sth1, then stripped and reprobed for anti-Rsc3 and anti-Rsc4. One of three technical replicates shown.
Figure 1- figure supplement 1. The Rsc3/30 module associates with the RSC1 complex at high stringency.
Figure 1- figure supplement 2. Additional swaps and truncations define the region of Rsc3/30 association.

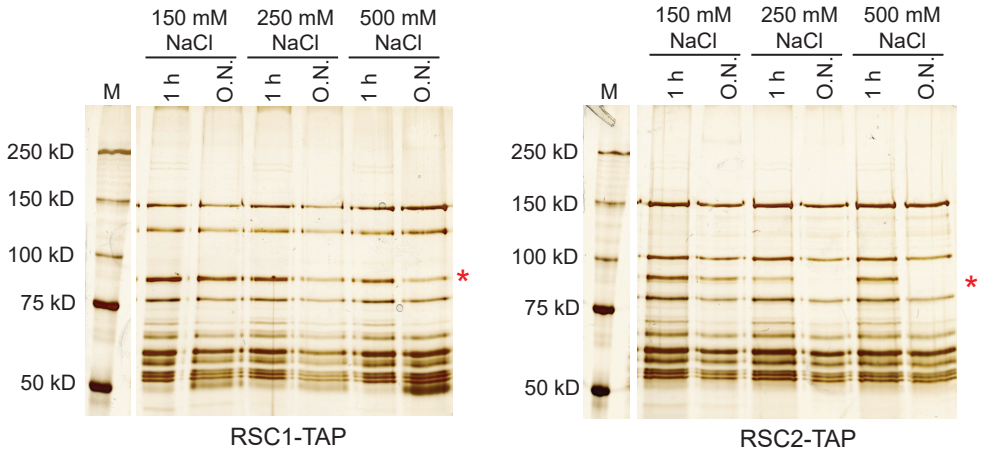

Figure 1 - figure supplement 1. The Rsc3/30 module associates with the RSC1 complex at high stringency. Yeast cell lysates containing RSC-TAP complexes were bound to IgG resin, the beads rinsed with lysis buffer before washing with buffer of the indicated salt concentration and duration. RSC complexes were analyzed on 6% acrylamide SDS-PAGE gels stained with silver. The Rsc3 and Rsc30 proteins run closely on denaturing gels and the doublet will often appear as a single band, marked by the asterisk (*). The marker lanes (M) are each from the adjacent gel, but were moved for depiction. Stringency testing conducted once.

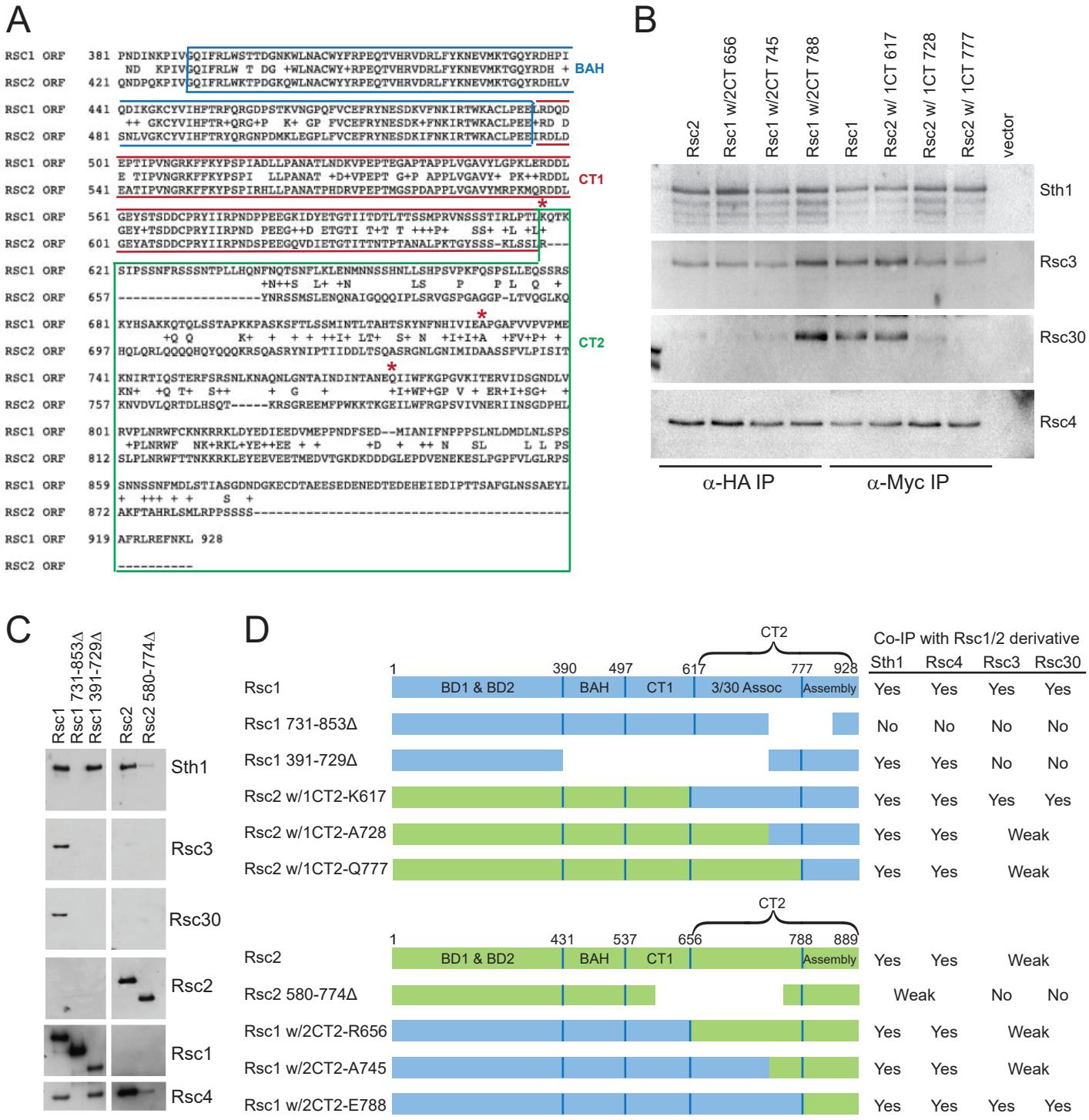

Figure 1 - figure supplement 2. Additional swaps and truncations define the region of Rsc3/30 association. (A) Alignment of C-terminus of Rsc1 and Rsc2, showing conservation and position of swaps (red asterisks). (B) Co-IPs of Rsc3 and Rsc30 with additional Rsc1 and Rsc2 CT swaps. Whole cell extracts prepared from *rsc1Δrsc2Δ* covered by *TRP1*-marked plasmid containing *RSC1*, *RSC2,* or CT swap were immunoprecipitated using anti-Myc (for CT2 of Rsc1), or anti-HA (for CT2 of Rsc2) bound to Dynabeads. Western blots were probed with antibodies against Sth1, Rsc3, Rsc30, and Rsc4. One of three biological replicates shown. (C) Co-IPs of RSC members with Rsc1 or Rsc2 containing deletions within the CT2 region. Whole cell extracts prepared from *rsc1Δrsc2Δ* covered by *TRP1*-marked plasmid containing deletions were immunoprecipitated using anti-Myc (for CT2 of Rsc1), or anti-HA (for CT2 of Rsc2) bound Dynabeads. Western blots were probed with antibodies against Sth1, Rsc3, Rsc30, Rsc2, Rsc4, and Myc. One of three technical replicates shown. (D) Summary of Rsc1 and Rsc2 Co-IPs from deletions and swaps.

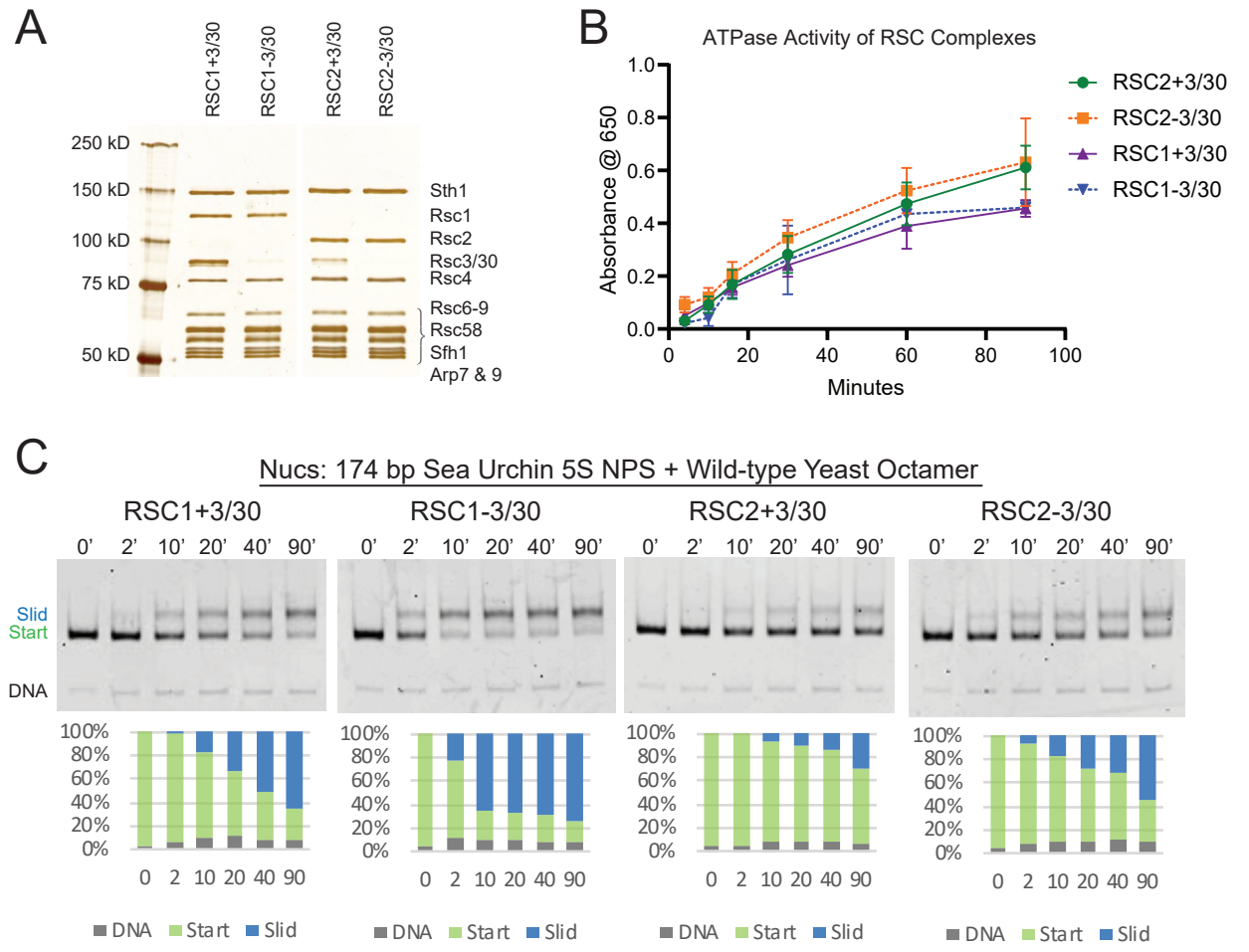

Figure 2. RSC1 and RSC2 complexes differ in remodeling activity on a sea urchin *5S* mononucleosomal substrate. (A) Alternative RSC1 and RSC2 complexes, with the Rsc3/30 module maintained or removed during purification. Purified RSC complexes (600 ng) were analyzed on 6% polyacrylamide SDS-PAGE gel stained with silver. The RSC1 and RSC2 complexes are from the same gel, but were moved adjacent for the depiction. (B) ATPase time course of RSC1 and RSC2 with and without the Rsc3/30 module. Values are the mean +/- standard deviation from two separate RSC preps for each RSC complex assayed in triplicate. (C) Comparative sliding of 174 bp sea urchin *5S* yeast mononucleosomes (20 nM) by RSC1 and RSC2 complexes (30 nM). The nucleosomal Start (green), Slid (blue), and free DNA (grey) bands were quantified and reported as a percent of the total signal.

Figure 2 - figure supplement 1. Quantification of RSC sliding 174 bp *5S* wild-type yeast mononucleosomes as conducted in Figure 2C.
Figure 2 - figure supplement 2. RSC complexes without Rsc3/30 module are ATP-dependent chromatin remodelers and RSC1 and RSC2 complexes bind similarly to 174 bp sea urchin *5S* mononucleosomes.
Figure 2 - figure supplement 3. The RSC *5S* sliding product is not the result of H2A/H2B dimer loss.

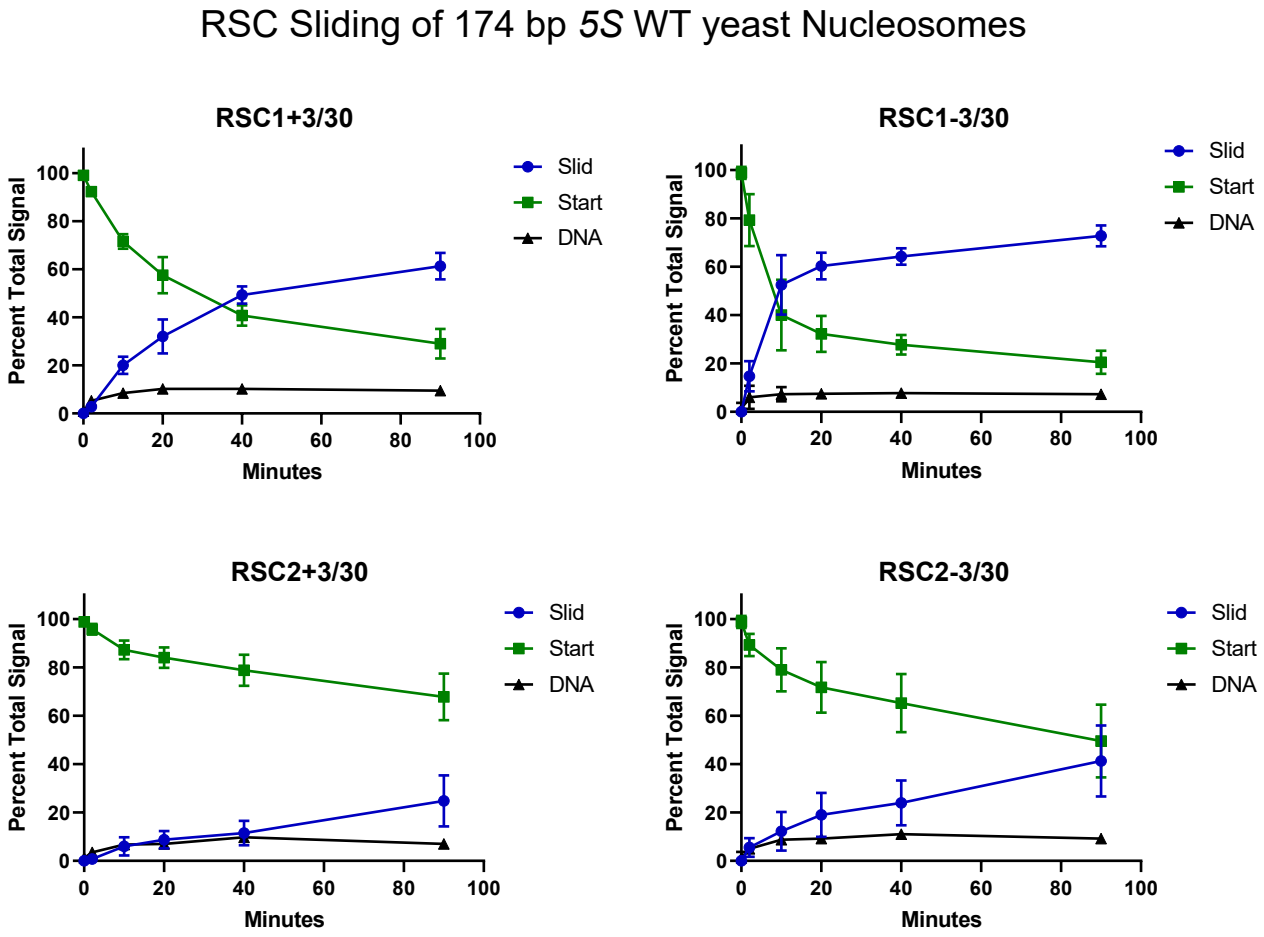

Figure 2 - figure supplement 1. Quantification of RSC sliding 174 bp *5S* wild-type yeast mononucleosomes as conducted in Figure 2C. Mean and standard deviation for four replicates.

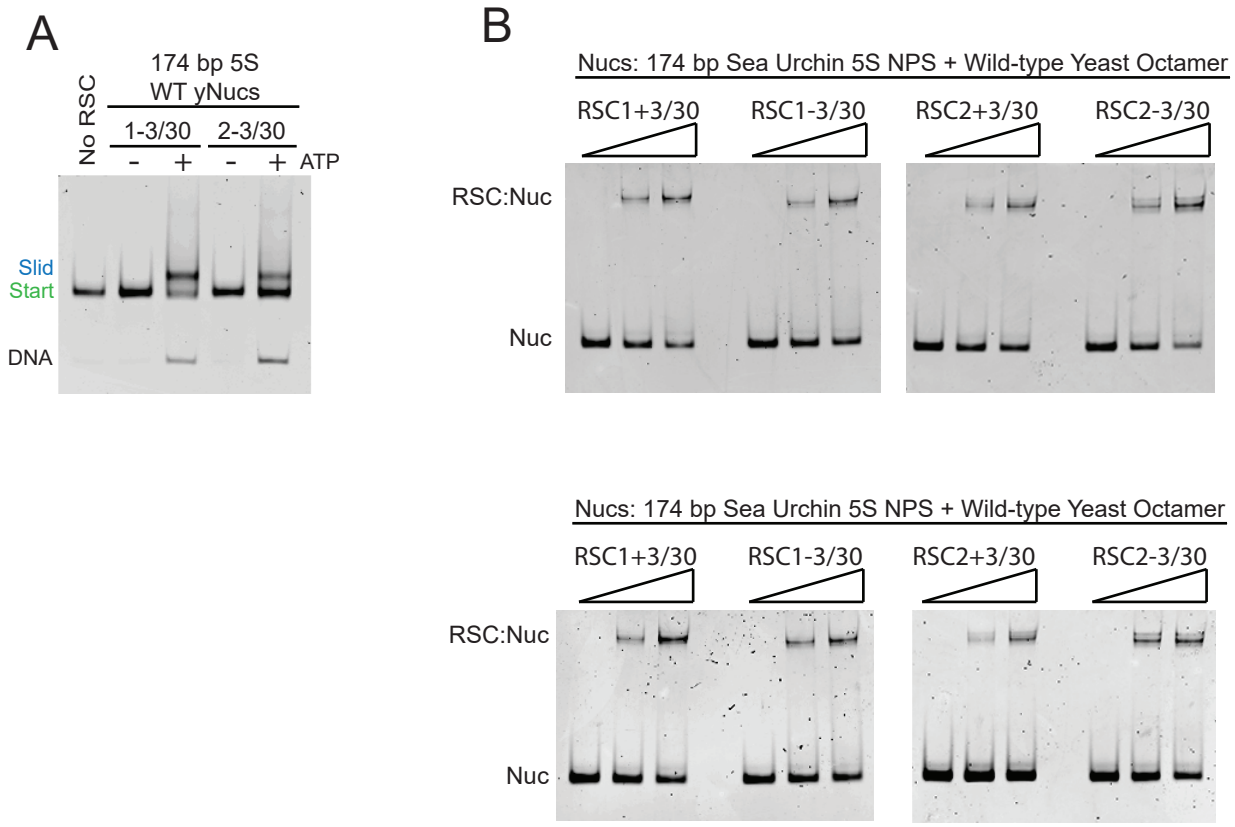

Figure 2 - figure supplement 2. RSC complexes without Rsc3/30 module are ATP-dependent chromatin remodelers and RSC1 and RSC2 complexes bind similarly to 174 bp sea urchin 5S mononucleosomes. (A) RSC1 and RSC2 complexes slide mononucleosomes in an ATP-dependent manner. Mononucleosomes (20 nM) were incubated in the presence (+) or absence (-) of 1 mM ATP with 30 nM of either the RSC1-3/30 (1-3/30) or the RSC2-3/30 (2-3/30) complex for 90 min at 30°C. Experiment conducted once. (B) RSC1 and RSC2 complexes bind similarly to mononucleosomes with 174 bp sea urchin *5S* DNA and wild-type yeast octamers. Nucleosomes (20 nM) were incubated with 0, 30, or 60 nM RSC for 20 min at 30˚C, run on a 3.8% native polyacrylamide gel, and stained with ethidium bromide. Two technical replicates shown.

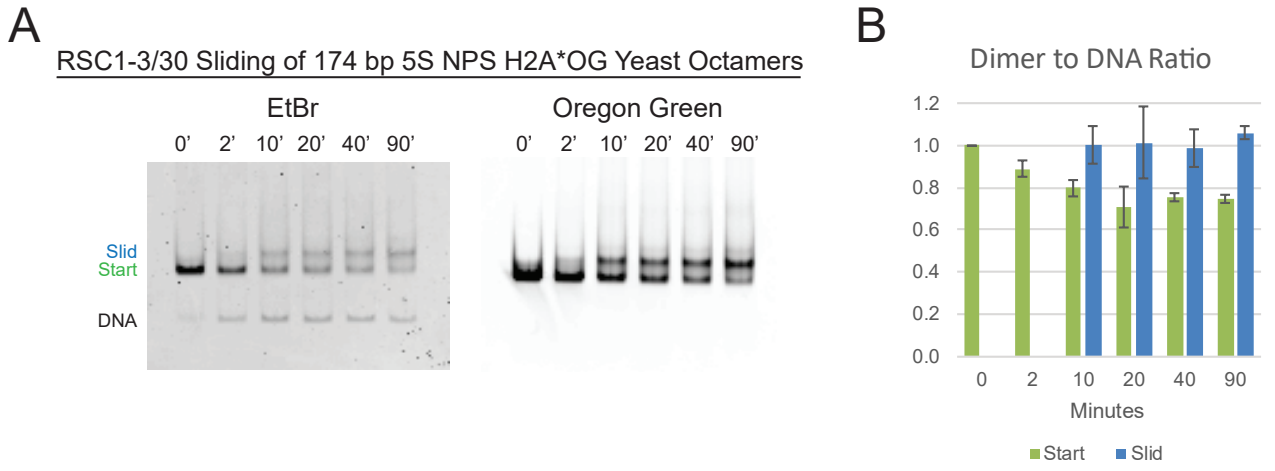

Figure 2 -figure supplement 3. The RSC *5S* sliding product is not the result of H2A/H2B dimer loss. (A) Nucleosome sliding by RSC1-3/30 (30 nM) of 174 bp sea urchin *5S* yeast mononucleosomes (20 nM) fluorescently labeled with Oregon Green (OG) on H2A (Q114C). The native gel was scanned for OG to detect the presence of H2A, followed by staining and scanning for ethidium bromide to detect DNA. (B) The ratio of H2A/H2B dimer to DNA was calculated for each of the Start and Slid bands and normalized to the starting nucleosomal band at the "0" time point. The average and standard deviation of sliding on two separate nucleosome preps were examined. The fluorescently labeled H2A*OG yeast octamers were a gift from L. McCullough and T. Formosa.

H3	1	2	3	4	5	6	7	8	9	10	11	12
A	R2A	T11A	L20A	T32A	R40A	R49A	S57A	L65A	E73A	L82A	L92A	V101A
B	T3A	G12A	S22A	G33A	Y41A	E50A	T58A	P66A	I74A	R83A	Q93A	S102A
C	K4A	G13A	K23A	G34A	K42A	I51A	E59A	F67A	Q76A	F84A	E94A	L103A
D	Q5A	K14A	R26A	V35A	P43A	R52A	L60A	Q68A	D77A	Q85A	S95A	F104A
E	T6A	P16A	K27A	K36A	G44A	R53A	L61A	R69A	F78A	S86A	V96A	E105A
F	R8A	R17A	S28A	K37A	T45A	F54A	I62A	L70A	K79A	S87A	E97A	D106A
G	K9A	K18A	P30A	P38A	V46A	Q55A	R63A	V71A	T80A	I89A	Y99A	T107A
H	S10A	Q19A	S31A	H39A	L48A	K56A	K64A	R72A	D81A	G90A	L100A	N108A
H3	1	2	3	4	5	6	7	8	9	10	11	12
A	L109A	Q120A	R129A									
B	I112A	K121A	L130A									
C	H113A	K122A	R131A									
D	K115A	D123A	G132A									
E	R116A	I124A	E133A									
F	V117A	K125A	R134A									
G	T118A	L126A	S135A									
H	I119A	R128A										
H4	1	2	3	4	5	6	7	8	9	10	11	12
A	S1A	G9A	H18A	I26A	R35A	K44A	E52A	F61A	S69A	R78A	V86A	R95A
B	G2A	L10A	R19A	Q27A	R36A	R45A	E53A	L62A	V70A	K79A	V87A	T96A
C	R3A	G11A	K20A	G28A	L37A	I46A	V54A	E63A	T71A	T80A	Y88A	L97A
D	G4A	K12A	I21A	I29A	R39A	S47A	R55A	S64A	Y72A	V81A	L90A	Y98A
E	K5A	G13A	L22A	T30A	R40A	G48A	V57A	V65A	T73A	T82A	K91A	G99A
F	G6A	G14A	R23A	K31A	G41A	L49A	L58A	I66A	E74A	S83A	R92A	F100A
G	G7A	K16A	D24A	P32A	G42A	I50A	K59A	R67A	H75A	L84A	Q93A	G101A
H	K8A	R17A	N25A	I34A	V43A	Y51A	S60A	D68A	K77A	D85A	G94A	G102A

Lethal w/ rsc1Δ | *Lethal w/ rsc2Δ* | *Lethal w/ rsc1Δ and rsc2Δ* | *Lethal in WT*

Table 1: Summary of Histone H3-H4 screen with *rsc1*Δ and *rsc2*Δ. Library of *TRP1*-marked plasmids containing H3-H4 residues mutated to alanine were transformed into *h3-h4*Δ [*H3-H4.URA3*] (YBC1939), *rsc1*Δ *h3-h4*Δ [*H3-H4.URA3*] (YBC2090) or *rsc2*Δ *h3-h4*Δ [*H3-H4.URA3*] (YBC3040), and spotted to SC-TRP, or SC-TRP+5FOA to force the loss of the wild type (WT) histone plasmid and test for synthetic lethality. Histone mutations that were lethal on their own in WT RSC are shaded grey, those that were lethal in combination with *rsc1*Δ are highlighted yellow, those that were lethal with *rsc2*Δ are highlighted in blue, and those residues that were lethal with *rsc1*Δ as well as with *rsc2*Δ are highlighted in green. Histone screen was performed one time and plasmids from lethal mutations were isolated and retransformed. Two or more transformants were tested to confirm phenotype.

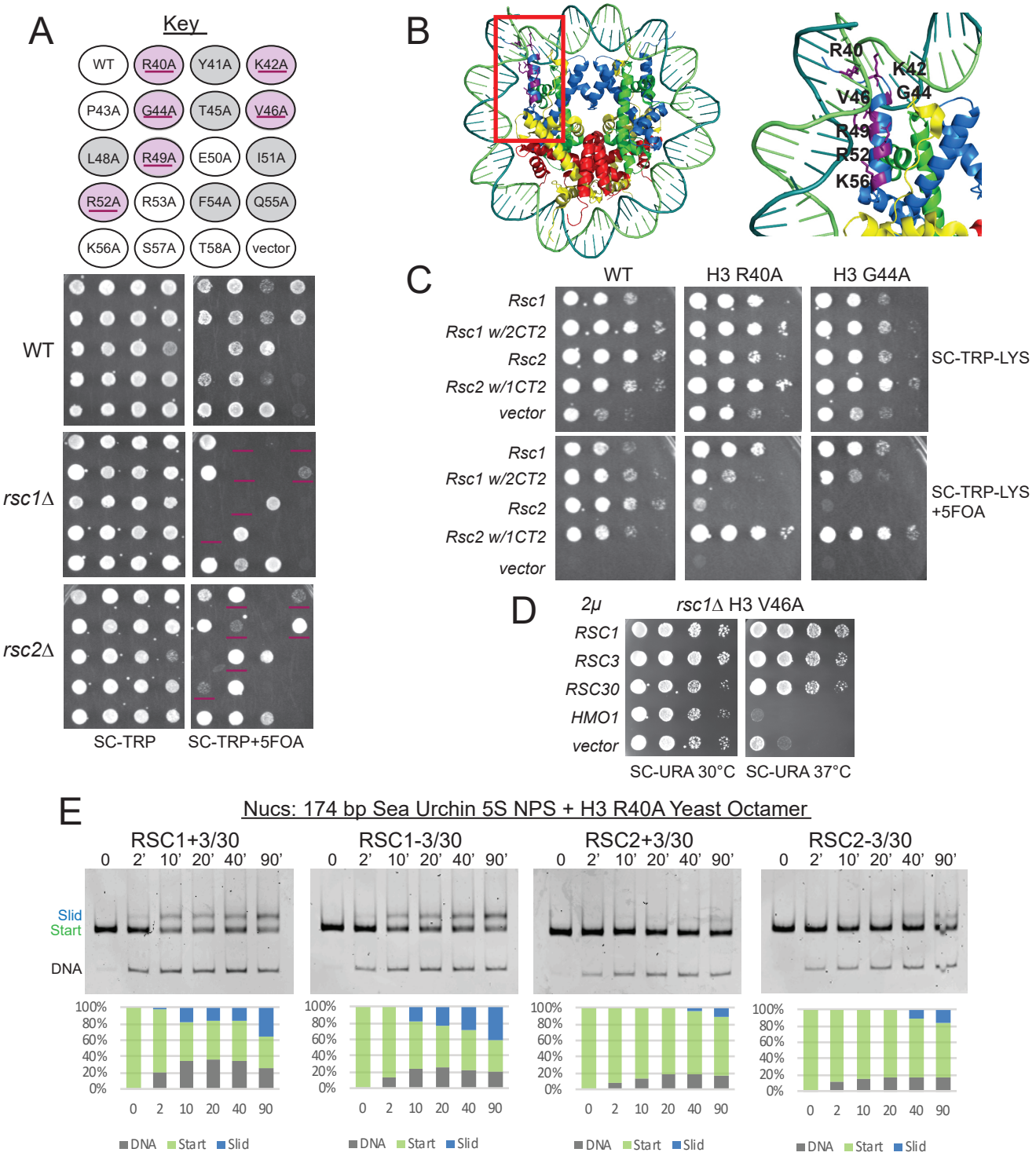

Figure 3. Mutations in the H3 αN helix are lethal in combination with r*sc1Δ*, but not *rsc2Δ*, and they reduce RSC remodeling of the *5S* nucleosome. (A) Histone H3 αN helix mutations that are lethal with *rsc1Δ*. *TRP1*-marked plasmids containing WT H4, and H3 mutations within the αN helix were transformed into *h3-h4Δ* [*H3-H4.URA3*] (YBC1939), *rsc1Δ h3-h4Δ* [*H3-H4.URA3*] (YBC2090) or *rsc2Δ h3-h4Δ* [*H3-H4.URA3*] (YBC3040), and spotted to SC-TRP or SC-TRP+5FOA to enforce the loss of the WT histone plasmid. Mutations that were lethal on their own without mutated RSC are shaded in grey. Mutations that were lethal in *rsc1Δ* but not *rsc2Δ* are shaded in purple and underlined. Transformants were grown at 30°C for 2 days. Shown is one of two biological replicates. (B) Location of the synthetic lethal *rsc1Δ* H3 αN helix mutations are depicted in purple on the nucleosome, PDB code 5NL0. (C) The *RSC1 CT2* region complements the synthetic lethal *rsc1Δ* H3 αN helix mutations. *rsc1Δ rsc2Δ h3-h4Δ* [*RSC1.URA3*] with [*H3.WT*, *R40A*, or *G44A-H4.WT. LYS2*] (YBC3466, YBC3444, YBC3433) transformed with *TRP1*-marked plasmids bearing *RSC1* (p609), *RSC2* (p604), *RSC1 w/2CT2* (p3097), *RSC2 w/1CT2* (p3098), or vector (pRS314) and spotted as 10x serial dilution to SC-TRP-LYS, or SC-TRP-LYS+5FOA. Shown is one of four biological replicates. (D) High-copy *RSC3* or *RSC30* will partially suppress the Ts⁻ phenotype of *rsc1Δ* H3V46A. Strain *rsc1Δ h3-h4Δ* [*H3.V46A-H4.WT.TRP*] (YBC3586) transformed with *URA3*-marked high copy (*2μ)* plasmids containing *RSC1* (p705), *RSC3* (p1310), *RSC30* (p916), *HMO1* (p3390), or vector (pRS426), and spotted as 10x serial dilutions at 30°C or 37°C. Shown is one of two biological replicates. (E) Comparative sliding and ejection of 174 bp sea urchin *5S* NPS H3 R40A yeast mononucleosomes (20 nM) by RSC1 and RSC2 complexes (30 nM). The nucleosomal Start (green), Slid (blue), and free DNA (grey) bands were quantified and reported as a percent of the total signal.

Figure 3 - figure supplement 1. Synthetic lethal mutations in each of the four histones H2A, H2B, H3 and H4 when combined with *rsc1Δ* or *rsc2Δ* mutations.

Figure 3 - figure supplement 2. Complementation by CT2 domain swaps when combined with H3 αN helix mutations.

Figure 3 - figure supplement 3. Quantification of RSC sliding 174 bp *5S* H3 R40A yeast mononucleosomes as conducted in Figure 3E.

Figure 3 - figure supplement 4. RSC1 and RSC2 complexes bind similarly to 174 bp sea urchin *5S* yeast mononucleosomes with the H3 R40A mutation.

Figure 3 - figure supplement 5. Mapping the positions of the wt and H3 R40A 174 bp sea urchin *5S* yeast mononucleosomes.

Mutation	* FRET %	Phenotype
WT	100 ± 6	No phenotype
R40A	71 ± 7	Lethal w/ rsc1Δ
Y41A	72 ± 7	Lethal w/ WT
K42A	54 ± 3	Lethal w/ rsc1Δ
P43A	91 ± 3	No phenotype
G44A	68 ± 9	Lethal w/ rsc1Δ
T45A	52 ± 5	Lethal w/ WT
V46A	89 ± 5	Lethal w/ rsc1Δ
L48A	86 ± 4	Lethal w/ WT
R49A	67 ± 3	Lethal w/ rsc1Δ
E50A	98 ± 6	No phenotype
I51A	81 ± 13	Lethal w/ WT
R52A	78 ± 3	Lethal w/ rsc1Δ
R53A	80 ± 4	No phenotype
F54A	96 ± 3	Lethal w/ WT
Q55A	69 ± 11	Lethal w/ WT
K56A	95 ± 4	No phenotype
S57A	102 ± 5	No phenotype
K56Q	82 ± 2	Lethal w/ rsc1Δ

* DNA end to end FRET,
from Ferreira et al, 2007

Table Supplement 1. DNA end to end FRET measurements on mononucleosomes containing H3 αN helix mutations from Ferreira et al, 2007 with the phenotype when combined with *RSC*, *rsc1Δ,* or *rsc2Δ*.

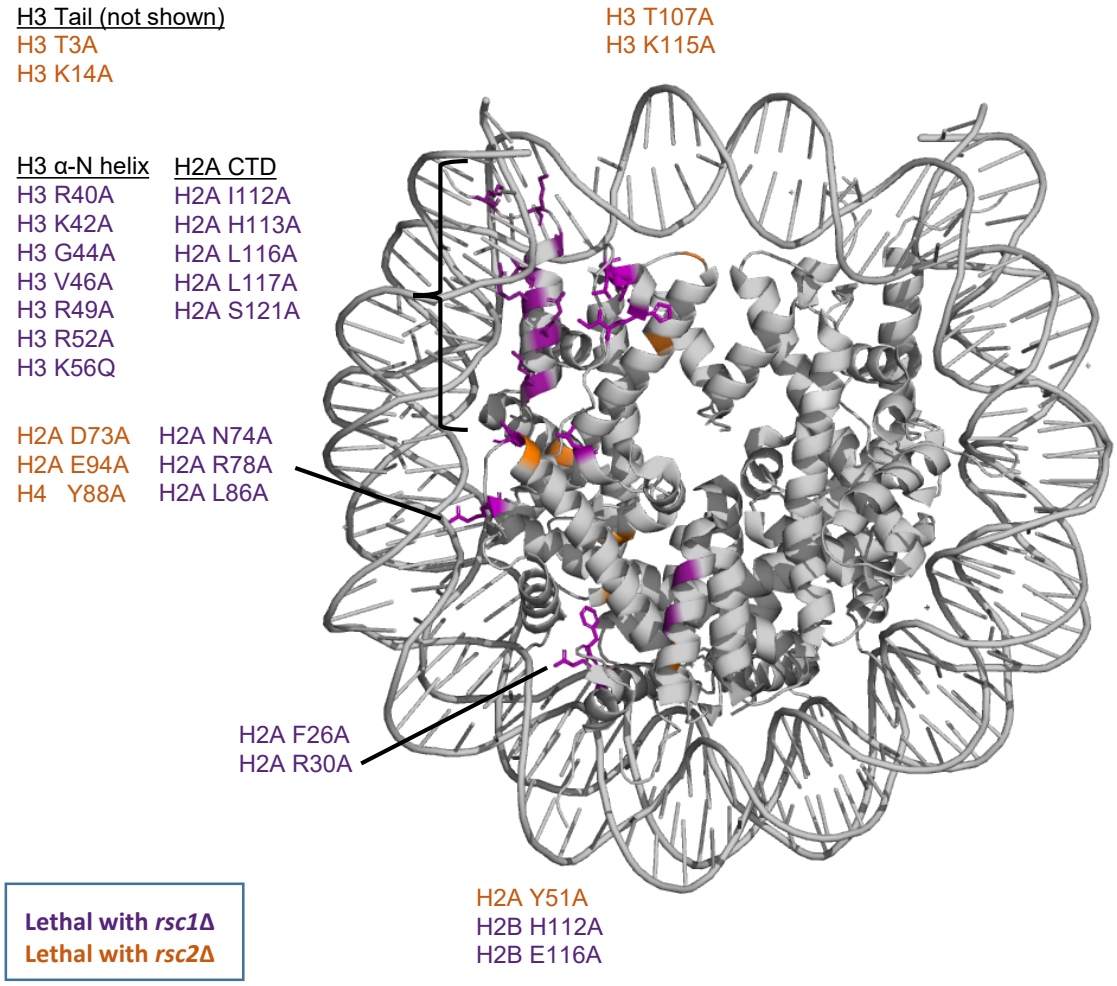

Figure 3- figure supplement 1. Synthetic lethal mutations in each of the four histones H2A, H2B, H3, and H4 when combined with *rsc1*Δ or *rsc2*Δ mutations. Mutations that are specifically lethal in combination with *rsc1*Δ are colored purple, mutations that are specifically lethal with *rsc2*Δ are colored orange. PDB code 1ID3.

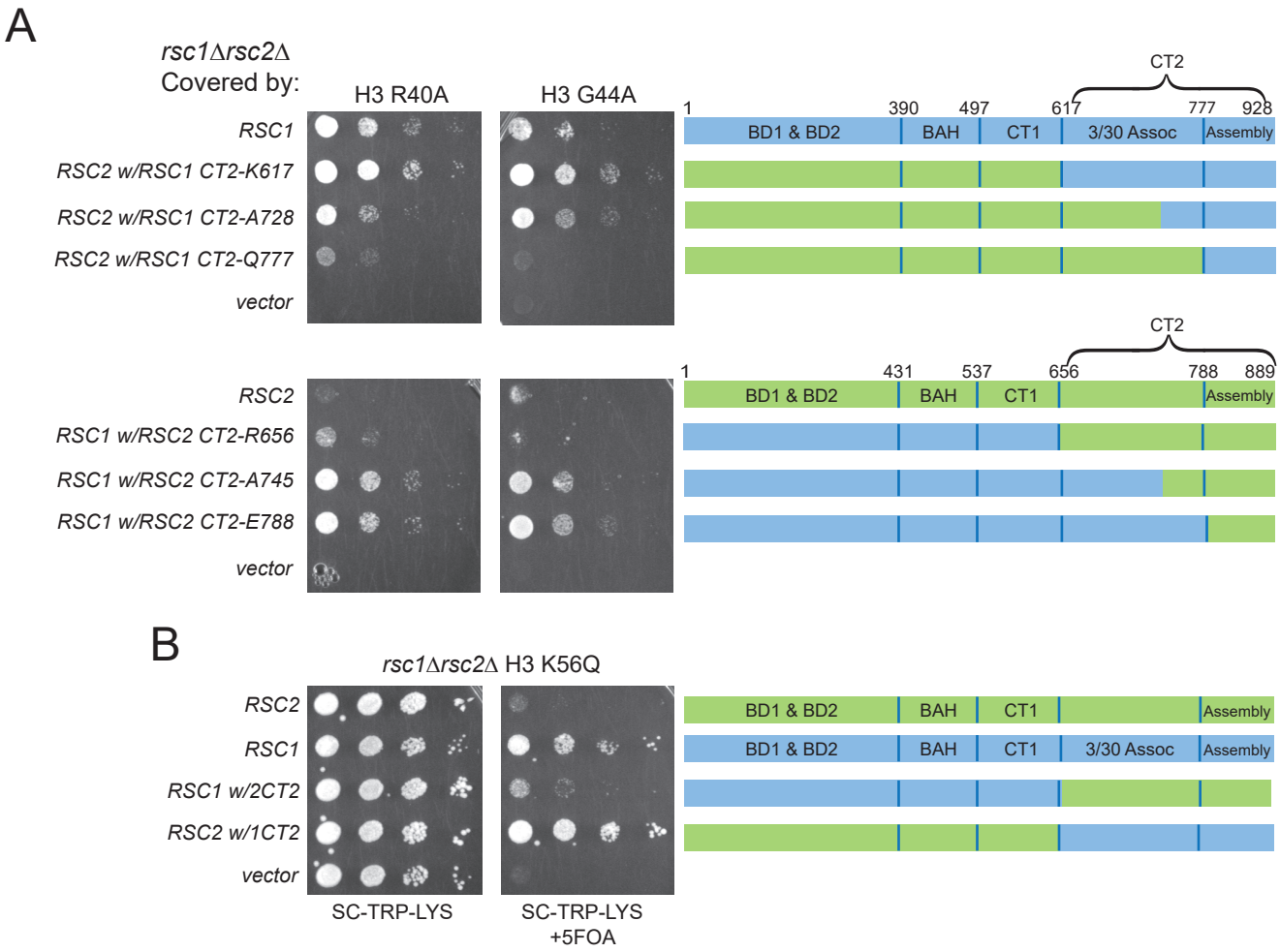

Figure 3 - figure supplement 2. Complementation by CT2 domain swaps when combined with H3 αN helix mutations. (A) The *RSC1 CT2* region complements the synthetic lethal *rsc1*Δ H3 αN helix mutations. Strain *rsc1*Δ *rsc2*Δ *h3-h4*Δ [*RSC1.URA3*] [*H3. R40A*, or *G44A-H4.WT. LYS2*] (YBC3444, YBC3433) transformed with *TRP1*-marked plasmids bearing *RSC1* (p609), *RSC2* (p604), C-Terminal swaps at positions noted (p3098, p3165, p3167, p3097, p3166, p3164) or vector (pRS314) and spotted as 10x serial dilution to SC-TRP-LYS, or SC-TRP-LYS+5FOA. One of four biological replicates shown. (B) Synthetic lethality of *rsc1*Δ H3 K56Q is complemented by the *RSC1 CT2* region. Strain *rsc1*Δ *rsc2*Δ *h3-h4*Δ [*RSC1.URA3*] [*H3.K56Q-H4.WT. LYS2*] (YBC3432) transformed with *TRP1*-marked plasmids bearing *RSC1* (p609), *RSC2* (p604), *RSC1 w/2CT2* (p3097), *RSC2 w/1CT2* (p3098), or vector (pRS314) and spotted as 10x serial dilution to SC-TRP-LYS, or SC-TRP-LYS+5FOA. One of four biological replicates shown.

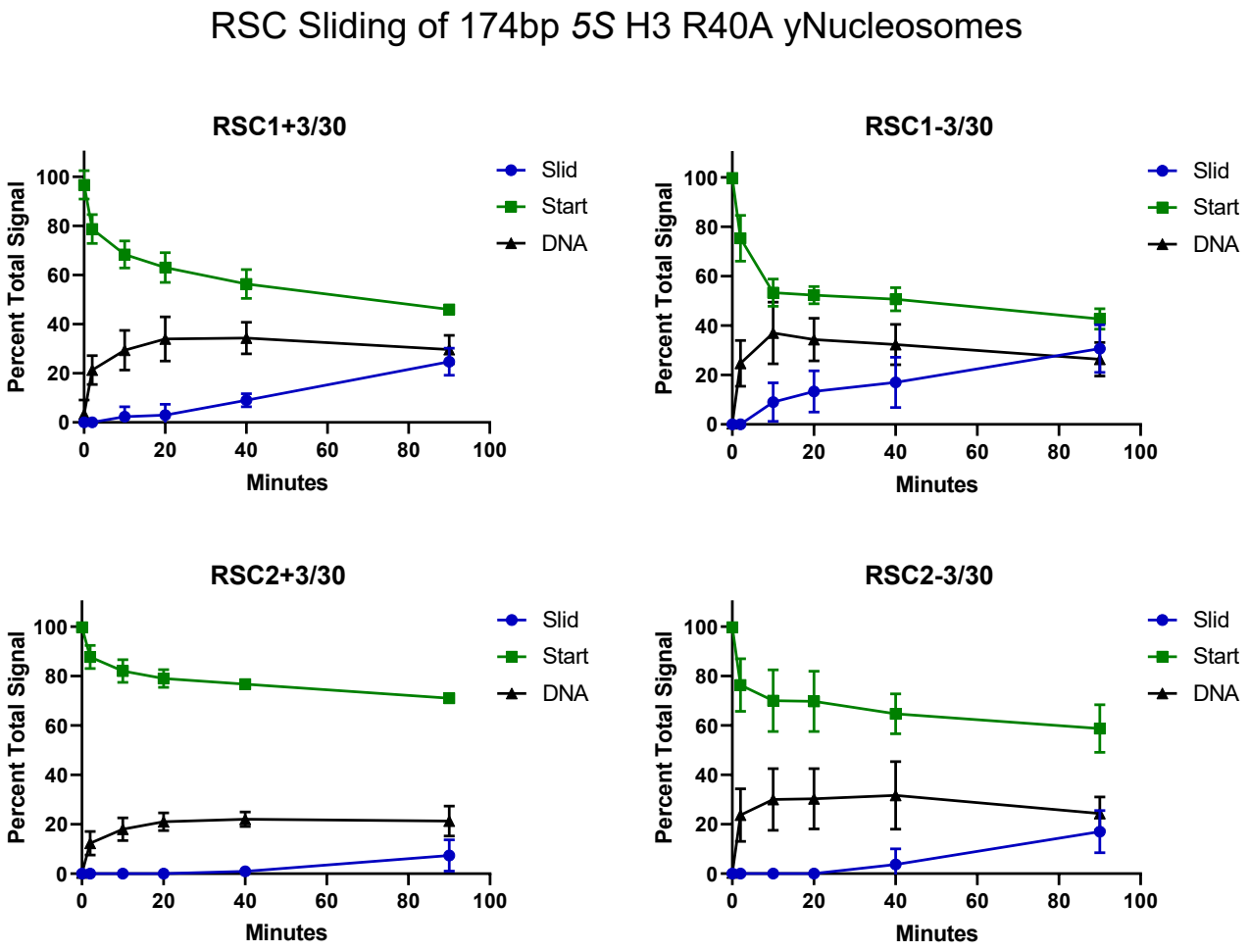

Figure 3 - figure supplement 3. Quantification of RSC sliding 174 bp *5S* H3 R40A yeast mononucleosomes as conducted in Figure 3E. Mean and standard deviation for three replicates.

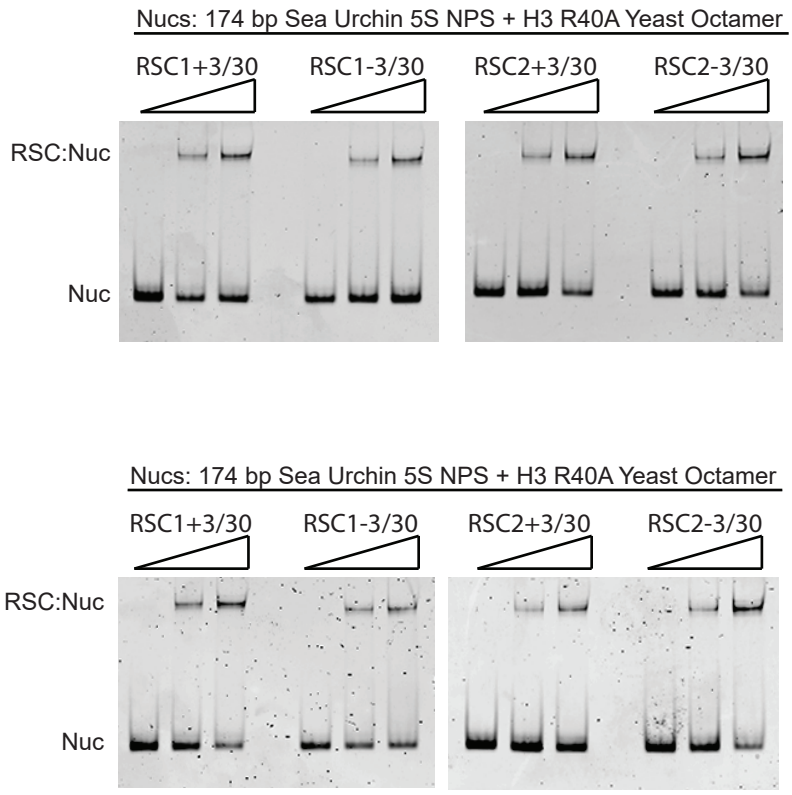

Figure 3 - figure supplement 4. RSC1 and RSC2 complexes bind similarly to 174 bp sea urchin *5S* yeast mononucleosomes with the H3 R40A mutation. Nucleosomes (20 nM) were incubated with 0, 30, or 60 nM RSC for 20 min at 30°C, run on a 3.8% native polyacrylamide gel, and stained with ethidium bromide. Two technical replicates shown.

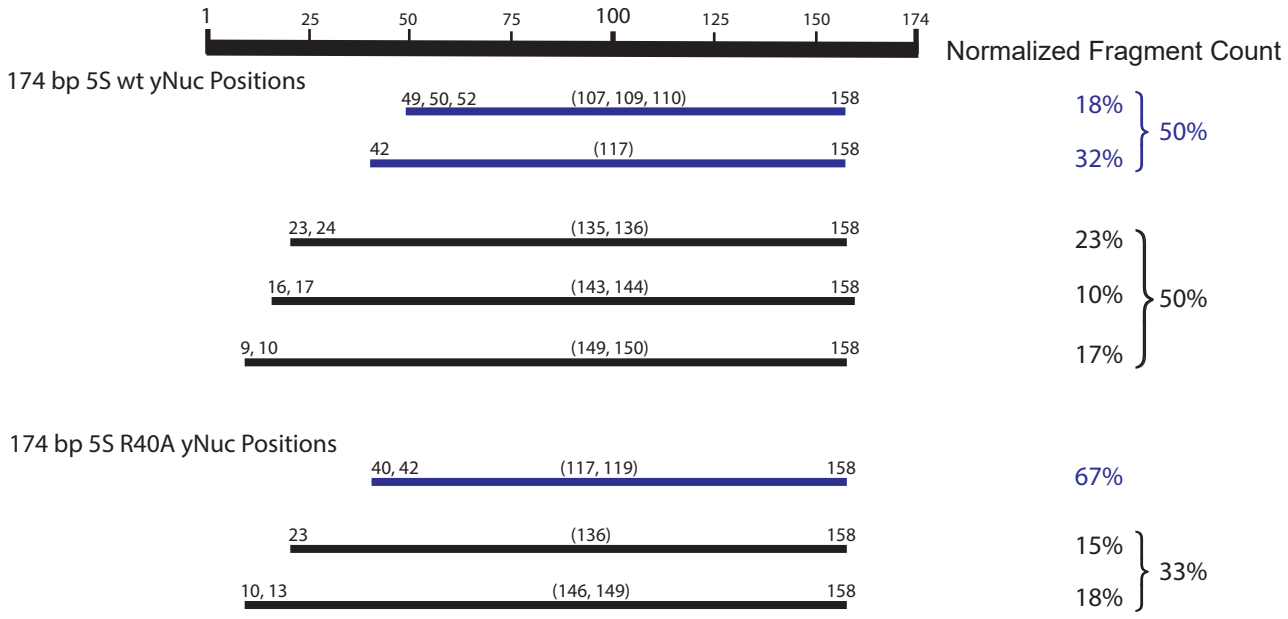

Figure 3 - figure supplement 5. Mapping the positions of the wt and H3 R40A 174 bp sea urchin *5S* yeast mononucleosomes. Nucleosome mapping by ExoIII and S1 treatment followed by paired-end next-generation sequencing. Experiment conducted once. Partially wrapped nucleosome fragments (≤120 bp) are depicted in blue. More fully wrapped nucleosome fragments (≥128 bp) are in black. Figure 3 - figure supplement 5 - Source Data 1. 174 bp *5S* nucleosome mapping.

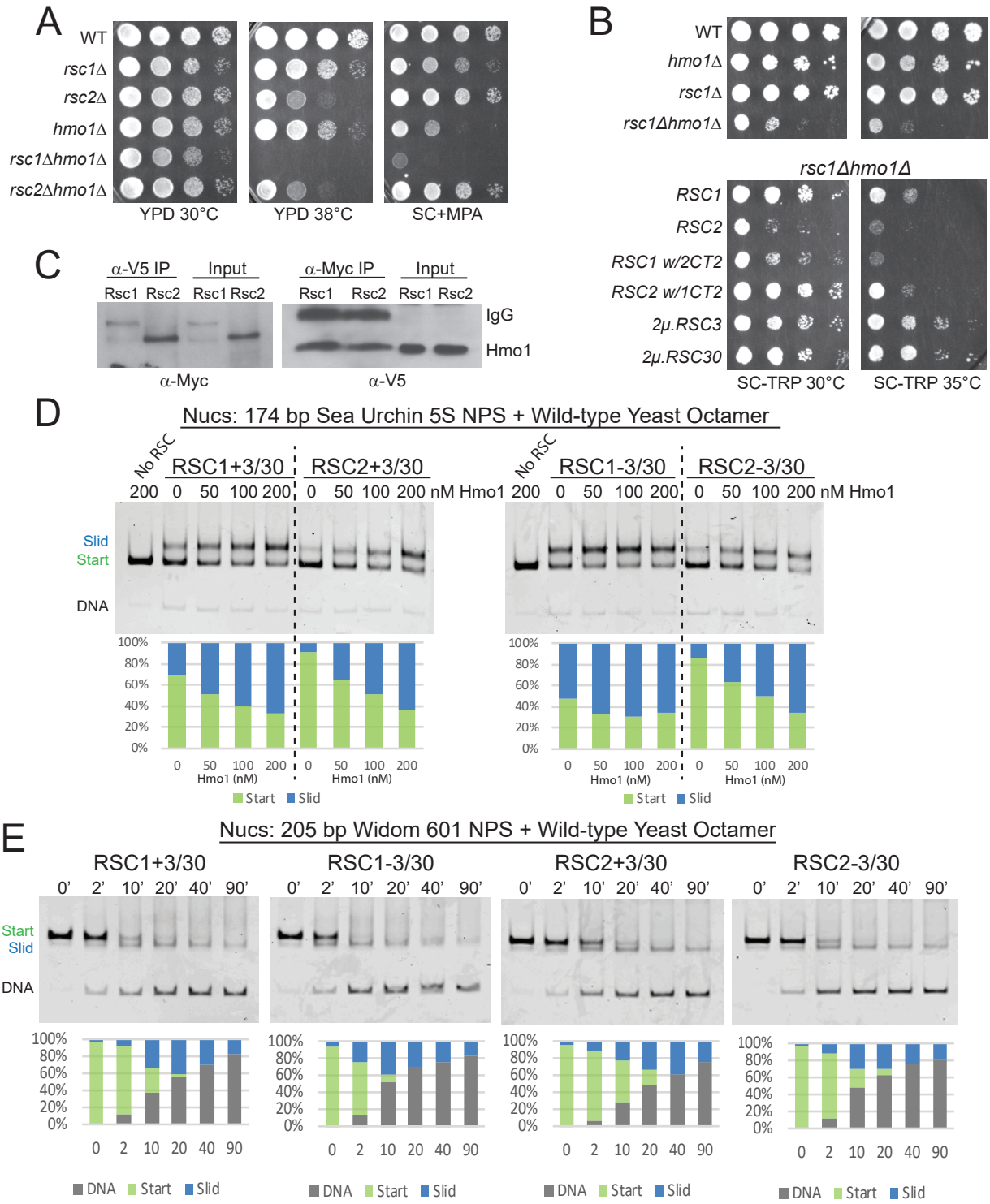

Figure 4. Hmo1 cooperates with RSC to remodel fragile or partially-unwrapped nucleosomes. (A) An *hmo1* null mutation is synthetically sick with *rsc1*Δ, but not *rsc2*Δ. WT (YBC604), *rsc1*Δ (YBC774), *rsc2*Δ (YBC82), *hmo1*Δ (YBC3509), *rsc1*Δ (YBC774), *rsc2*Δ (YBC82), *rsc1*Δ *hmo1*Δ (YBC3514), *rsc2*Δ *hmo1*Δ (YBC3515) spotted as 10x serial dilutions to YPD 30°C, YPD 38°C, and SC+20 μg/ml mycophenolic acid (MPA). One of two or more biological replicates shown. (B) The *rsc1*Δ *hmo1*Δ synthetic sickness is suppressed by high copy *RSC3*, *RSC30*, or *RSC1 CT2*. Strain *rsc1*Δ *hmo1*Δ (YBC3514) transformed with *TRP1*-marked *RSC1* (p609), *RSC2* (p604), *RSC1 w/2CT2* (p3097), *RSC2 w/1CT2* (p3098), *2μ.RSC3* (p929), *2μ.RSC30* (p911), or vector (pRS314) spotted as 10x serial dilutions to SC-TRP 30°C or SC-TRP 35°C. One of four biological replicates shown. (C) Co-IP of Rsc1 and Rsc2 with Hmo1. Sonicated chromatin extracts from *RSC1.9XMYC HMO1.V5* (YBC3558) and *RSC2.9XMYC HMO1.V5* (YBC3559) were immunoprecipitated using anti-Myc or anti-V5. Western blots were probed with anti-Myc or anti-V5 antibodies. One of three biological replicates shown. (D) Comparative sliding by RSC1 and RSC2 complexes (10 nM) of 174 bp sea urchin *5S* yeast mononucleosomes (20 nM) pre-incubated with increasing concentrations of Hmo1 protein. Reactions were conducted at 30°C for 20 min. The Start (green) and Slid (blue) bands were quantified and reported as percent of the total signal. The free DNA band was negligible and not quantified. (E) Comparative sliding and ejection of Widom 601 yeast mononucleosomes (20 nM) by RSC1 and RSC2 complexes (10 nM). The nucleosomal Start (green), Slid (blue), and free DNA (grey) bands were quantified and reported as a percent of the total signal.

Figure 4 - figure supplement 1. Co-immunoprecipitation of Rsc1 and Rsc2 with Hmo1 from MNase-treated chromatin extracts.

Figure 4 - figure supplement 2. Quantification of Hmo1 stimulation of RSC sliding 174 bp 5S wild-type yeast mononucleosomes as conducted in Figure 4D.

Figure 4 - figure supplement 3. Additional sliding assays and quantification of 174 bp *5S* yeast mononucleosomes with RSC and Hmo1.

Figure 4 - figure supplement 4. Quantification of RSC sliding 205 bp Widom 601 wild-type yeast mononucleosomes as conducted in Figure 4E.

Figure 4 - figure supplement 5. RSC1 and RSC2 slide Widom 601 H3 R40A mononucleosomes similarly.

Figure 4 - figure supplement 6. Quantification of RSC sliding 205 bp Widom 601 H3 R40A yeast mononucleosomes as conducted in Figure 4 - figure supplement 5A.

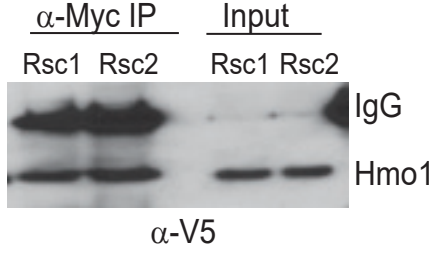

Figure 4- figure supplement 1. Co-Immunoprecipitation of Rsc1 and Rsc2 with Hmo1 from MNase-treated chromatin extracts. *RSC1.9XMYC HMO1.V5* (YBC3558) and *RSC2.9XMYC HMO1.V5* (YBC3559) were immunoprecipitated using anti-Myc bound dynabeads. 100% of Co-IP and 5% of input were loaded on the gel. Western blots were probed with anti-V5 antibody. One of three biological replicates shown.

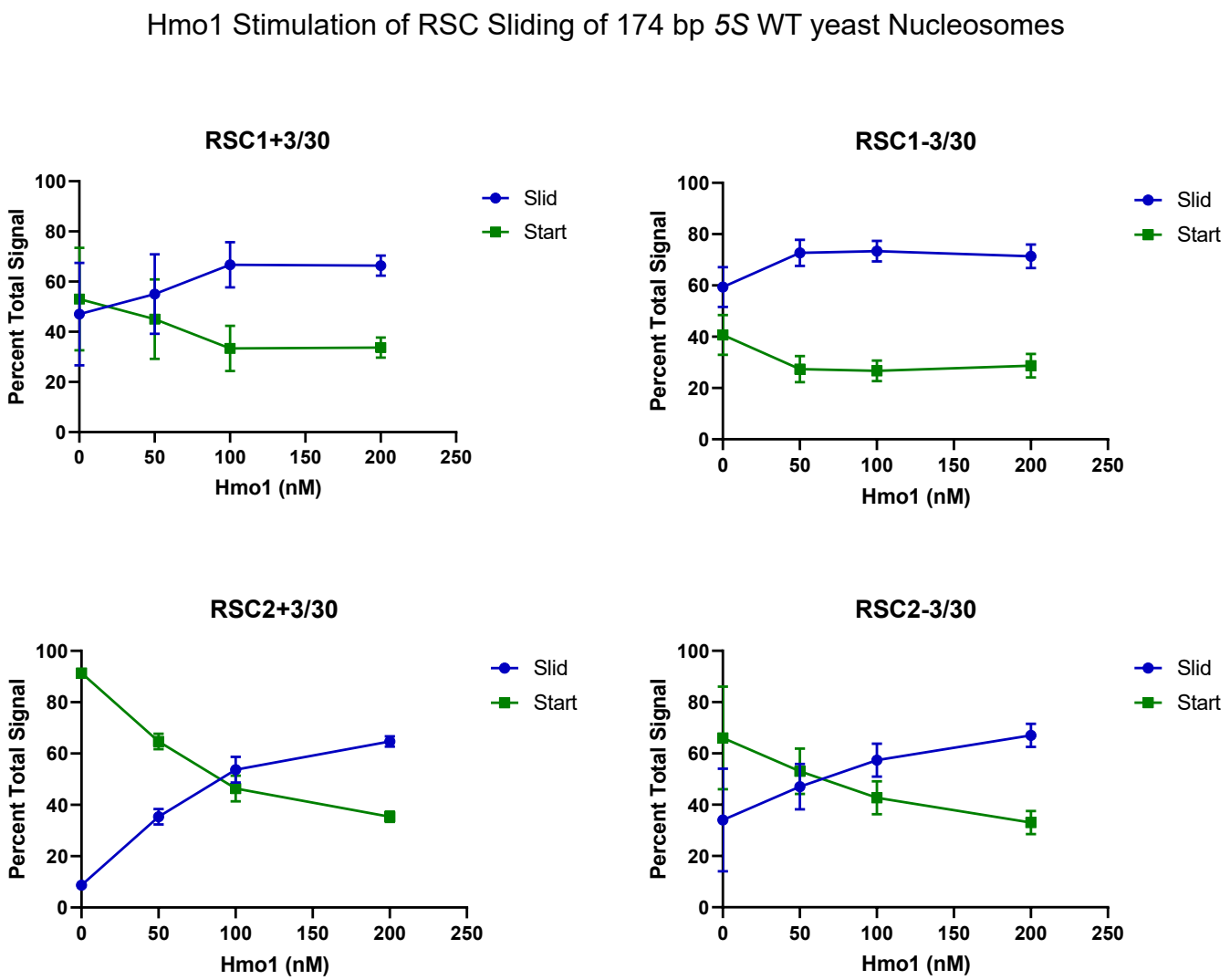

Figure 4 - figure supplement 2. Quantification of Hmo1 stimulation of RSC sliding 174 bp *5S* wild-type yeast mononucleosomes as conducted in Figure 4D. Mean and standard deviation for three replicates.

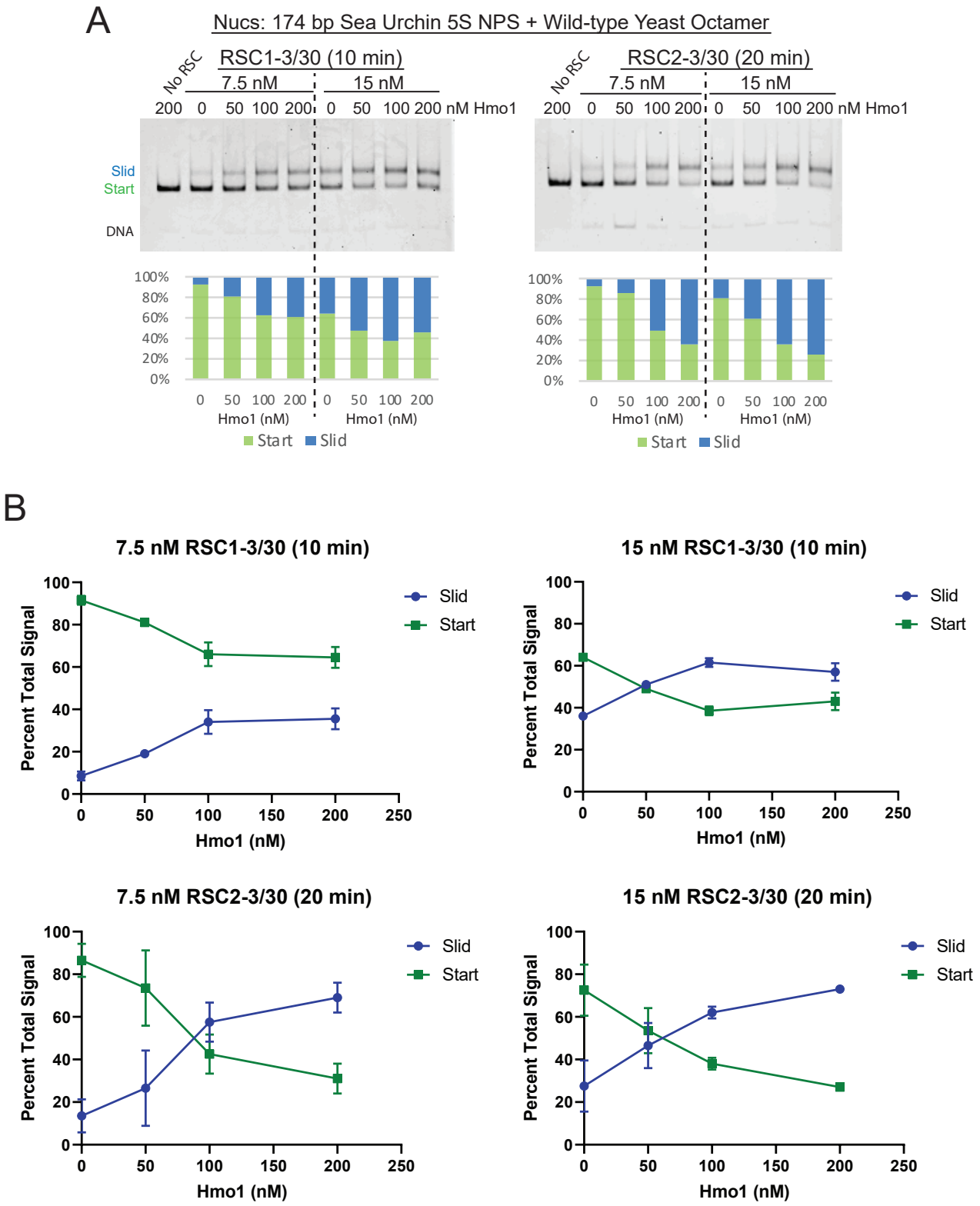

Figure 4 - figure supplement 3. Additional sliding assays and quantification of 174 bp *5S* yeast mononucleosomes with RSC and Hmo1. (A) 174 bp *5S* yeast mononucleosomes (20 nM) were pre-incubated with increasing concentrations of Hmo1. RSC concentrations and reaction times are as indicated. All reactions were conducted at 30°C. The Start (green) and Slid (blue) bands were quantified and reported as percent of the total signal. The free DNA band was negligible and not quantified. (B) Quantification of Hmo1 stimulation of RSC sliding 174 bp *5S* wild-type yeast mononucleosomes. Mean and standard deviation for two replicates

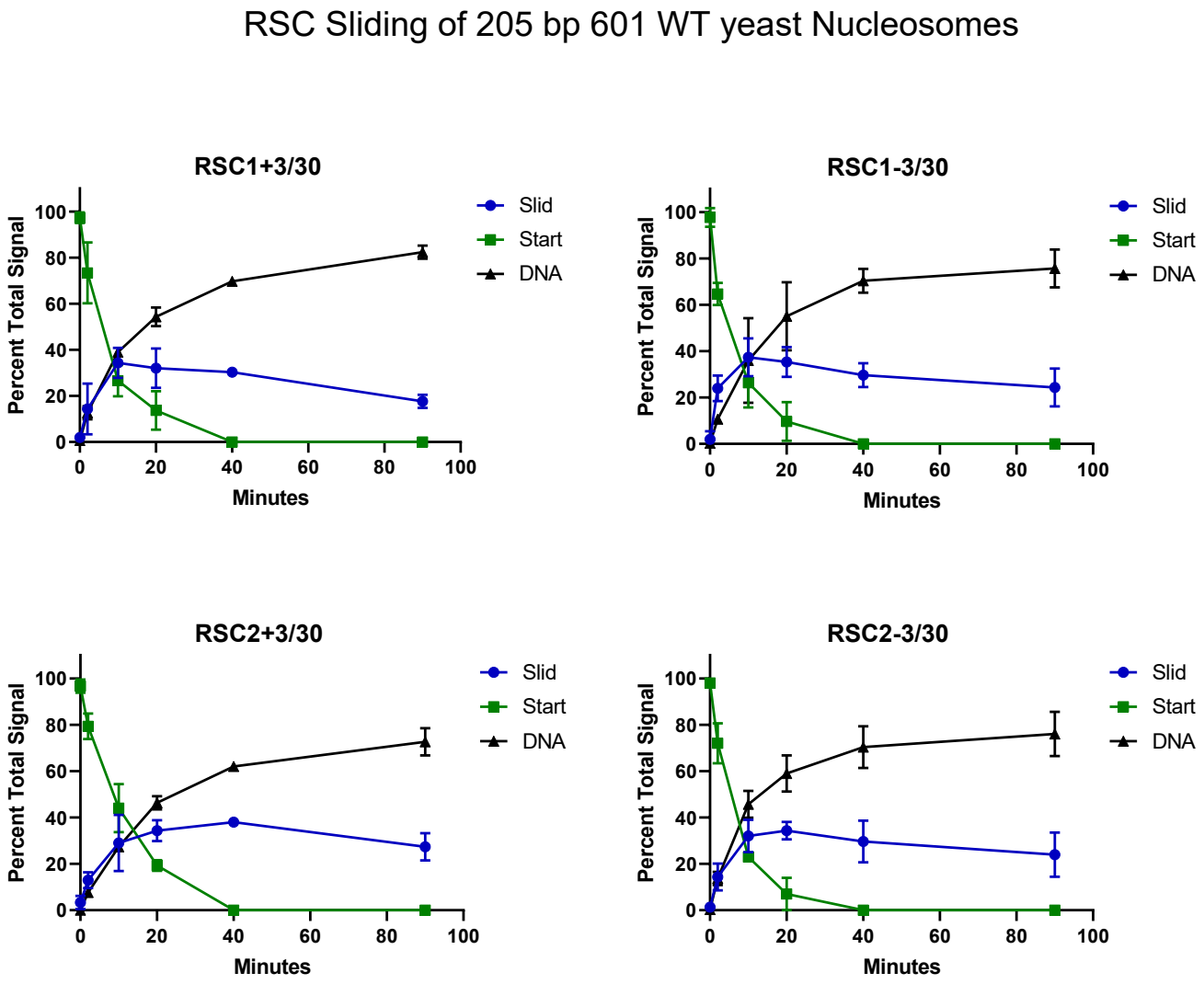

Figure 4 - figure supplement 4. Quantification of RSC sliding 205 bp Widom 601 wild-type yeast mononucleosomes as conducted in Figure 4E. Mean and standard deviation for three replicates.

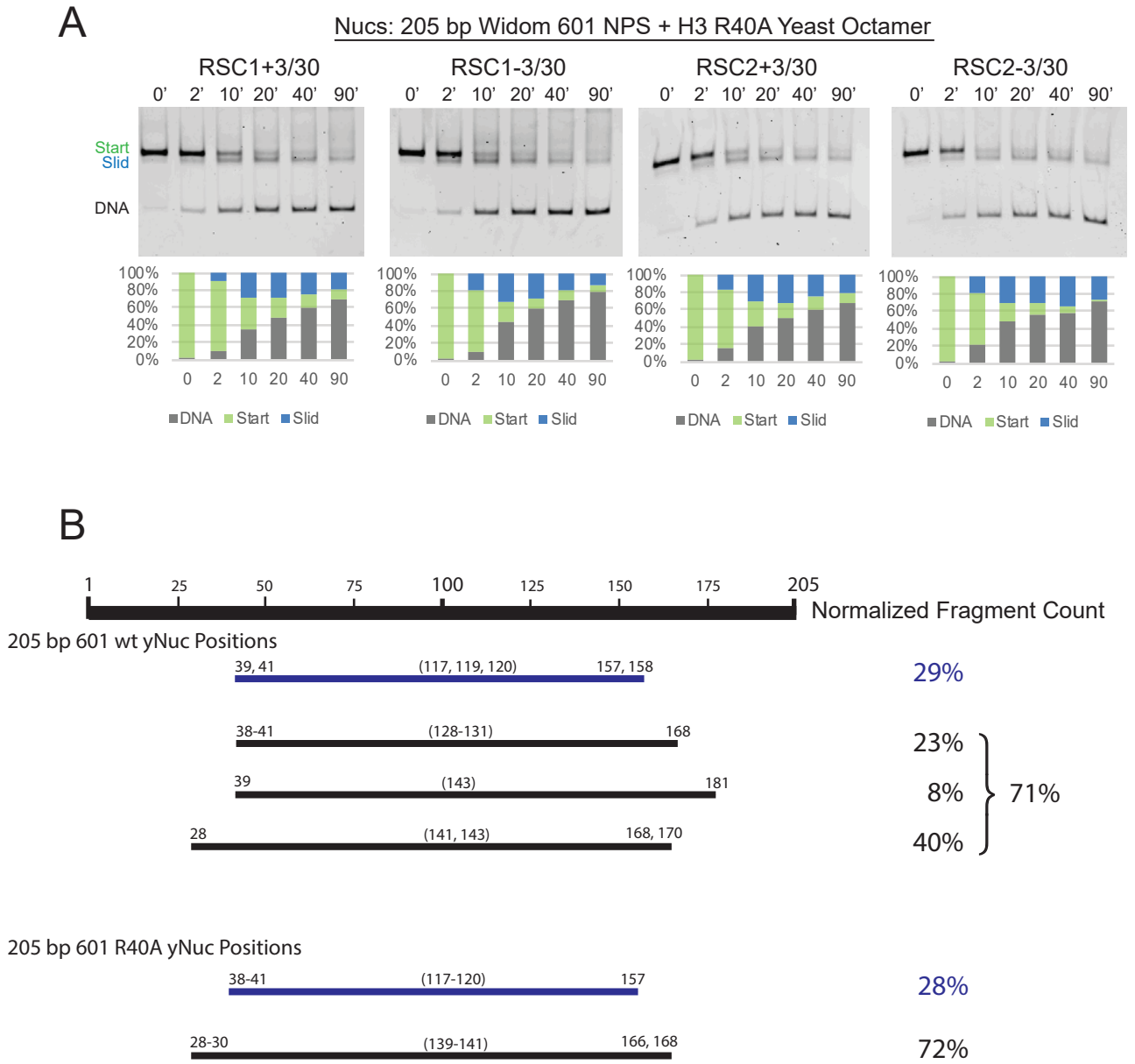

Figure 4 - figure supplement 5. RSC1 and RSC2 slide Widom 601 H3 R40A mononucleosomes similarly. (A) Comparative sliding of RSC1 and RSC2 complexes (10 nM) on H3 R40A 205 bp Widom 601 yeast mononucleosomes (20 nM). The nucleosomal Start (green), Slid (blue), and free DNA (grey) bands were quantified and reported as a percent of the total signal. (B) Mapping the positions of the wild-type and H3 R40A 205 bp Widom 601 yeast mononucleosomes by ExoIII and S1 treatment as in Figure 3 -figure supplement 3. Partially unwrapped nucleosome fragments (≤120 bp) are depicted in blue. More fully wrapped nucleosome fragments (≥128 bp) are in black. Averages from two technical replicates.
Figure 4 - figure supplement 5B - Source Data 1. 205 bp Widom 601 nucleosome mapping.

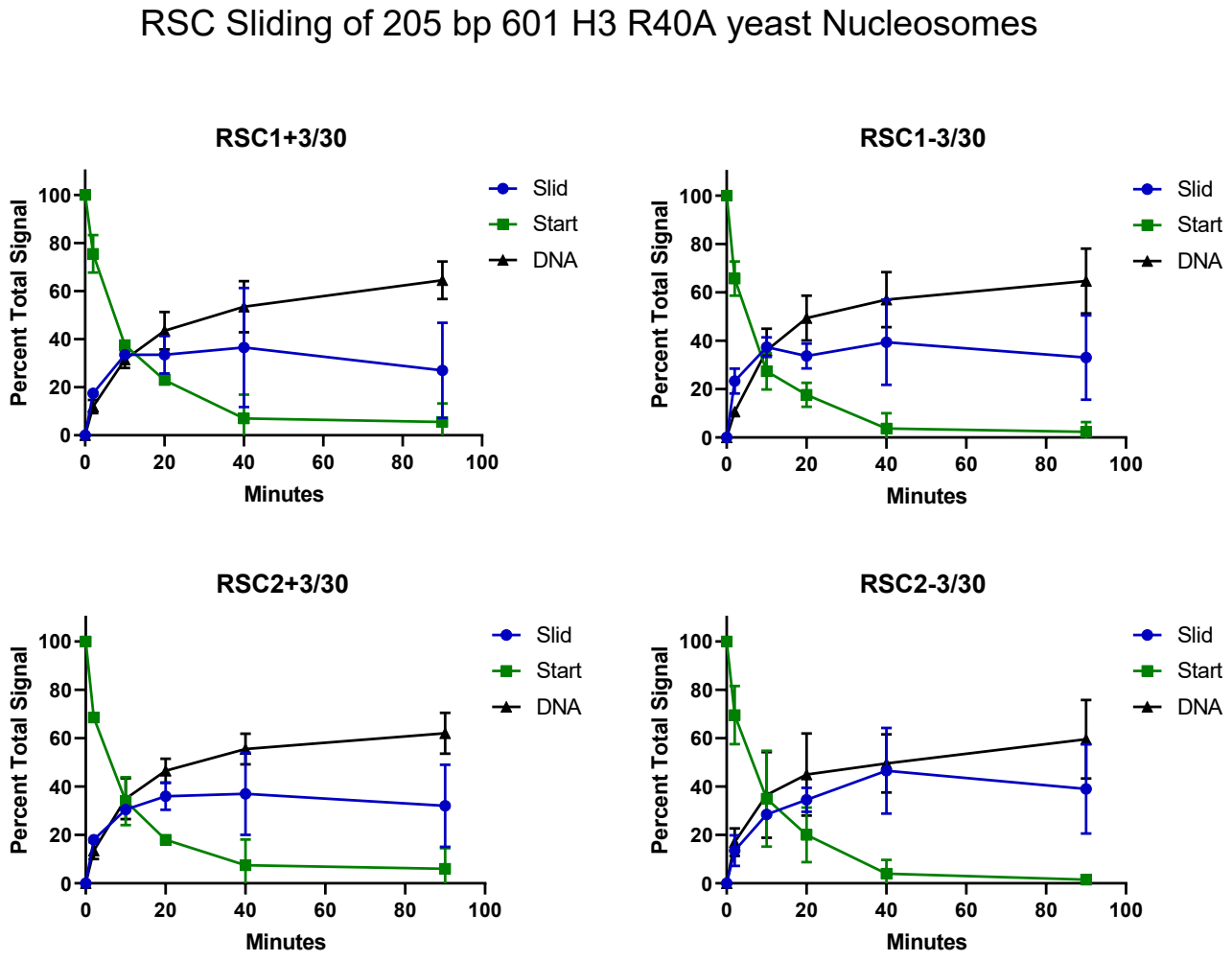

Figure 4 - figure supplement 6. Quantification of RSC sliding 205 bp Widom 601 H3 R40A yeast mononucleosomes as conducted in Figure 4 - figure supplement 5A. Mean and standard deviation for two replicates.

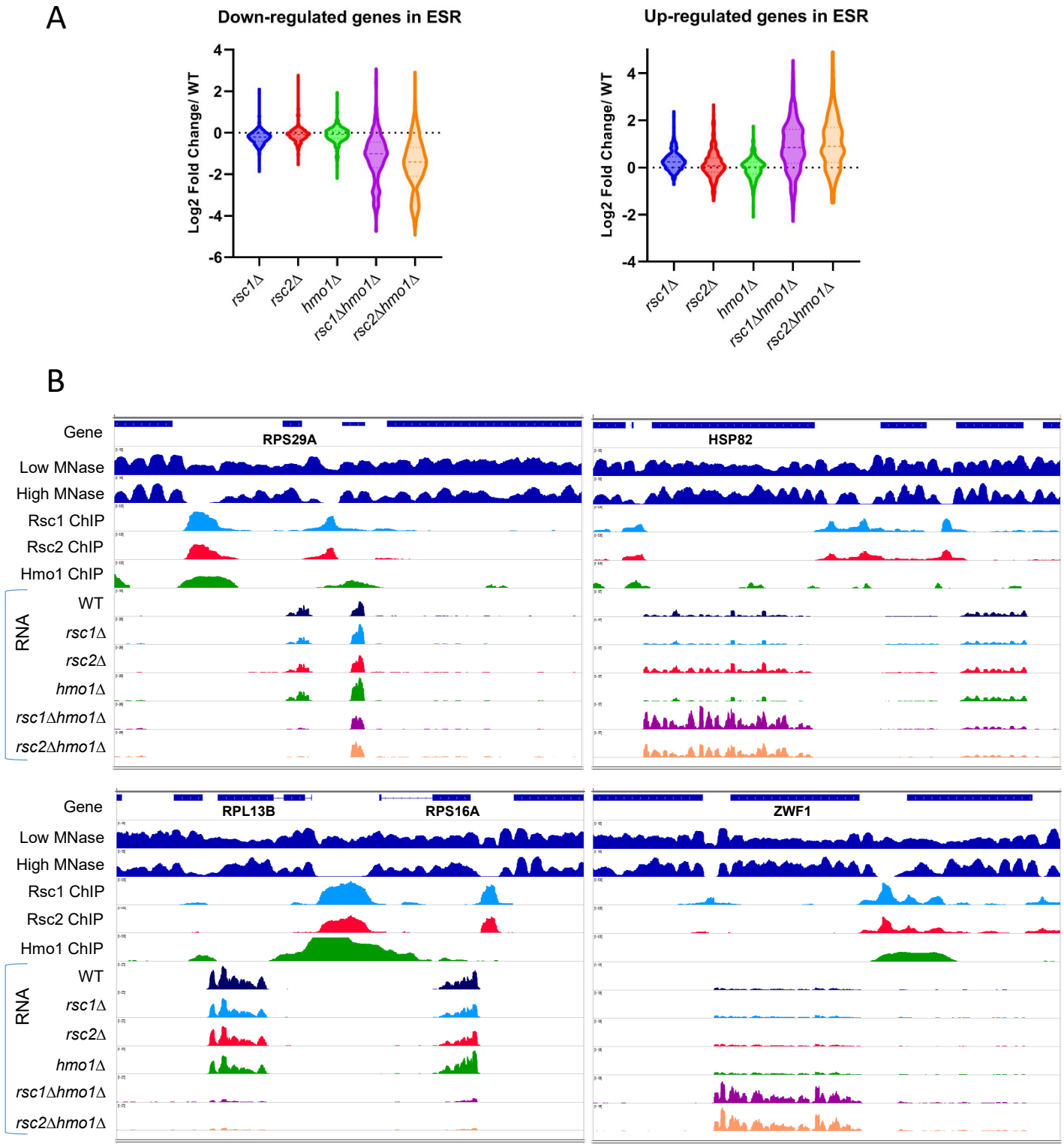

Figure 5- figure supplement 1. Gene expression changes in *rsc1*Δ, *rsc2*Δ, and *hmo1*Δ mutants.
(A) The effect of *rsc* deletions on genes involved in the environmental stress response (ESR). Violin plot showing expression changes (average of three biological replicates) in *rsc* mutants for genes that are up-regulated (255 genes) or down regulated (587 genes) in the ESR (Gasch et al, 2000). (B) Genome Snapshots. Shown for select genes are low- (GSM1891202) and high- (GSM1891207) MNase digested fragment coverage from Kubik et al, 2015, Rsc1 and Rsc2 ChIP Seq log2 fold enrichments, Hmo1 ChIP Seq log2 fold enrichment (GSM1509041) from Knight et al, 2014, RNASeq coverage (unstranded) from an average of three biological replicates of RNAseq for WT(YBC604), *rsc1*Δ (YBC774), *rsc2*Δ (YBC82), *hmo1*Δ (YBC3509), *rsc1*Δ *hmo1*Δ (YBC3514), *rsc2*Δ *hmo1*Δ (YBC3515).
Figure 5- figure supplement 1- Source Data 1. List of ESR affected genes.

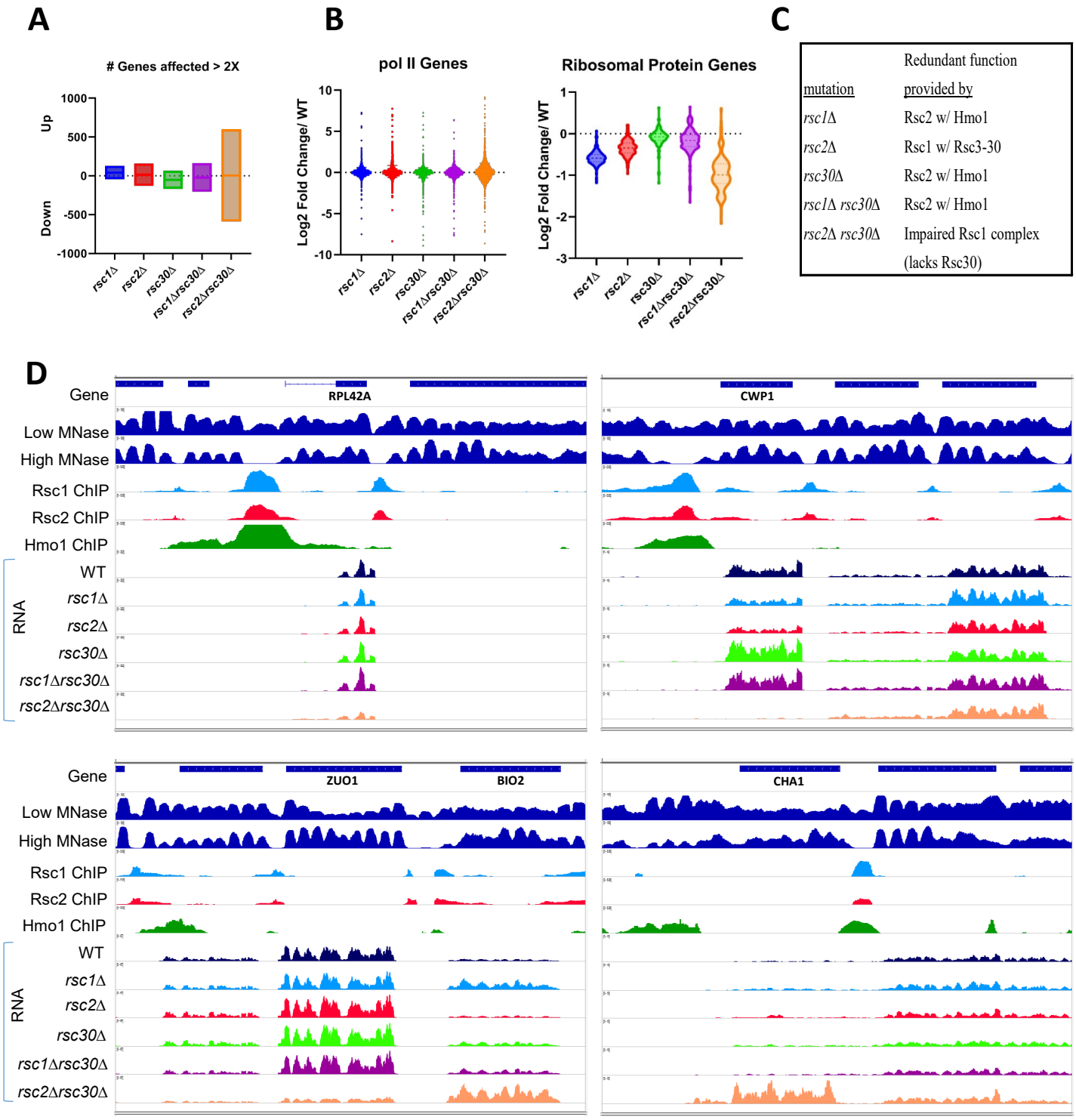

mutation	Redundant function provided by
rsc1Δ	Rsc2 w/ Hmo1
rsc2Δ	Rsc1 w/ Rsc3-30
rsc30Δ	Rsc2 w/ Hmo1
rsc1Δ rsc30Δ	Rsc2 w/ Hmo1
rsc2Δ rsc30Δ	Impaired Rsc1 complex (lacks Rsc30)

Figure 5 – figure supplement 2: Gene expression changes in *rsc1*Δ, *rsc2*Δ, and *rsc30*Δ mutants. (A) Number of genes affected by *rsc* deletions. For each mutation, the number of genes up or downregulated two fold or more compared to WT. *rsc1*Δ (↑129↓45), *rsc2*Δ (↑160↓129), *rsc30*Δ (↑66↓168), *rsc1*Δ*rsc30*Δ (↑162↓204), *rsc2*Δ*rsc30*Δ (↑601↓589). (B) Gene Expression changes. Violin plots showing log2 fold change of RNA in mutants at all pol II genes (6145 genes) and at ribosomal protein genes (132 genes) compared to WT expression. Change in expression reflects an average of three biological replicates, Figure 5- Source Data 3. (C) Rsc mutation redundancy relationship. (D) Genome snapshots. Shown for select genes are low- (GSM1891202) and high- (GSM1891207) MNase-digested fragment coverage from Kubik et al, 2015, Rsc1 and Rsc2 ChIP seq log2 fold enrichments, Hmo1 ChIP Seq log2 fold enrichments (GSM1509041) from Knight et al, 2014, and RNASeq coverage (unstranded) from an average of three replicates of RNAseq for WT (YBC604), *rsc1*Δ (YBC774), *rsc2*Δ (YBC82), *rsc30*Δ (YBC695), *rsc1*Δ *rsc30*Δ (YBC839), and *rsc2*Δ *rsc30*Δ (YBC910).

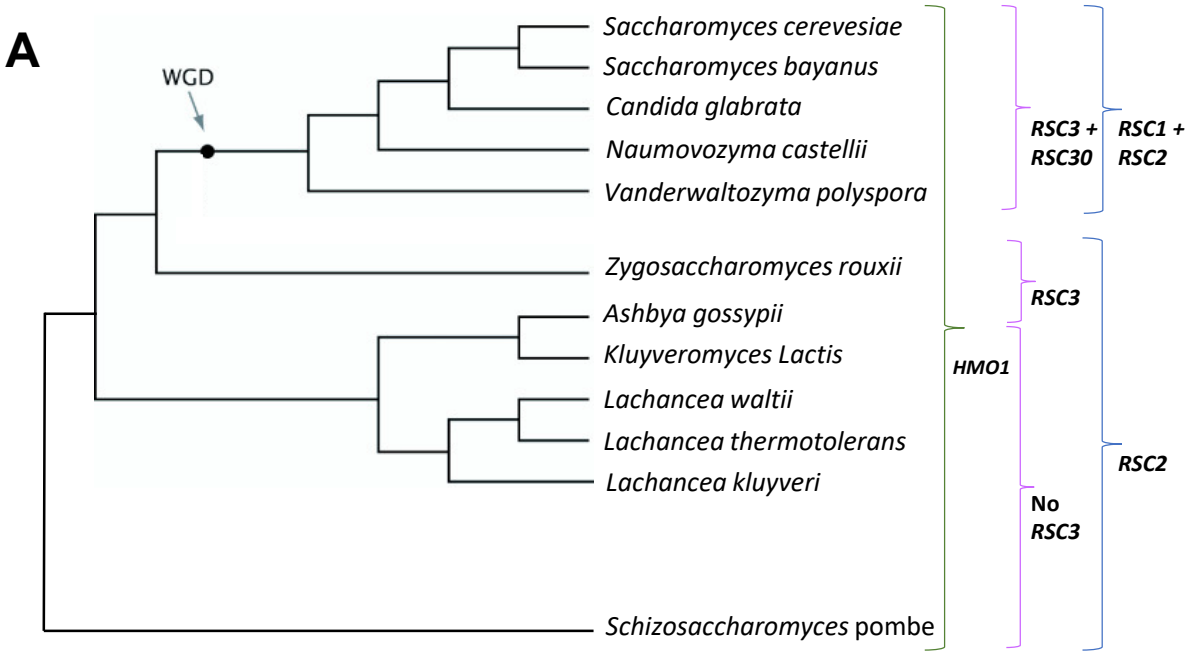

B

Yeast Species	Rsc1/2 ortholog protein identifier	Rsc2 score	Rsc2 E value	Rsc1 score	Rsc1 E value
Candida glabrata *	CAG57994.1	794	0	637	0
Candida glabrata *	CAG61377.1	695	0	762	0
Naumovozyma castelii *	XP_003673169.1	788	0	698	0
Naumovozyma castelii *	XP_003678436.1	704	0	651	0
Vanderwaltozyma polyspora *	XP_001643414.1	718	0	770	0
Vanderwaltozyma polyspora *	XP_001643343.1	621	0	583	0
Zygosaccharomyces rouxii	ZYRO0B07986p	875	0	805	0
Ashbya gossypii	ABL005Cp	751	0	687	0
Lachancea thermotolerans	XP_002551602.1	785	0	711	0
Kluyveromyces lactis	CAH025113.1	501	2E-163	506	8E-165
Candida albicans	EEQ42885.1	405	3E-128	398	4E-125
Yarrowia lipolytica	XP_503084.1	316	5E-95	288	2E-84
Schizosaccharomyces pombe	CAA19283.1	224	1E-62	223	4E-62

Yeast Species	Rsc3/30 ortholog protein identifier	Rsc3 score	Rsc3 E value	Rsc30 score	Rsc30 E value
Candida glabrata *	CAG59797.1	389	5E-123	113	3E-36
Candida glabrata *	CAG58494.1	149	2E-37	100	4E-22
Naumovozyma castelii *	XP_003677109.1	532	2E-177	143	1E-35
Naumovozyma castelii *	XP_003673610.1	75.1	2E-14	77.8	4E-15
Vanderwaltozyma polyspora *	XP_001646730.1	495	2E-163	103	3e-323
Vanderwaltozyma polyspora *	XP_001642773.1	358	4E-111	119	5E-28
Zygosaccharomyces rouxii	ZYRO0C13882p	577	0	127	2E-30
Ashbya gossypii	AAL057Cp	400	1E-126	97.1	7E-21
Lachancea thermotolerans	No significant ortholog				
Kluyveromyces lactis					
Candida albicans					
Yarrowia lipolytica					
Schizosaccharomyces pombe					

Figure 5- supplement 3. (A) Appearance of *RSC1/RSC2* and *RSC3/RSC30* in yeast evolution. Phylogenetic tree adapted from OhÉigeartaigh et al, 2011 with the appearance of *RSC1/RSC2*, and *RSC3/RSC30.* WGD refers to whole genome duplication. Duplication of *RSC2* and *RSC3* resulted in *RSC1* and *RSC30* in *S. cerevisiae*. While the duplicated genes in other organisms may still more closely resemble *RSC2* or *RSC3*, *RSC1* and *RSC30* have been used to indicate the duplicated copy. (B) Scores from NCBI Fungal Blast for *RSC1/RSC2* and *RSC3/RSC30* orthologs.

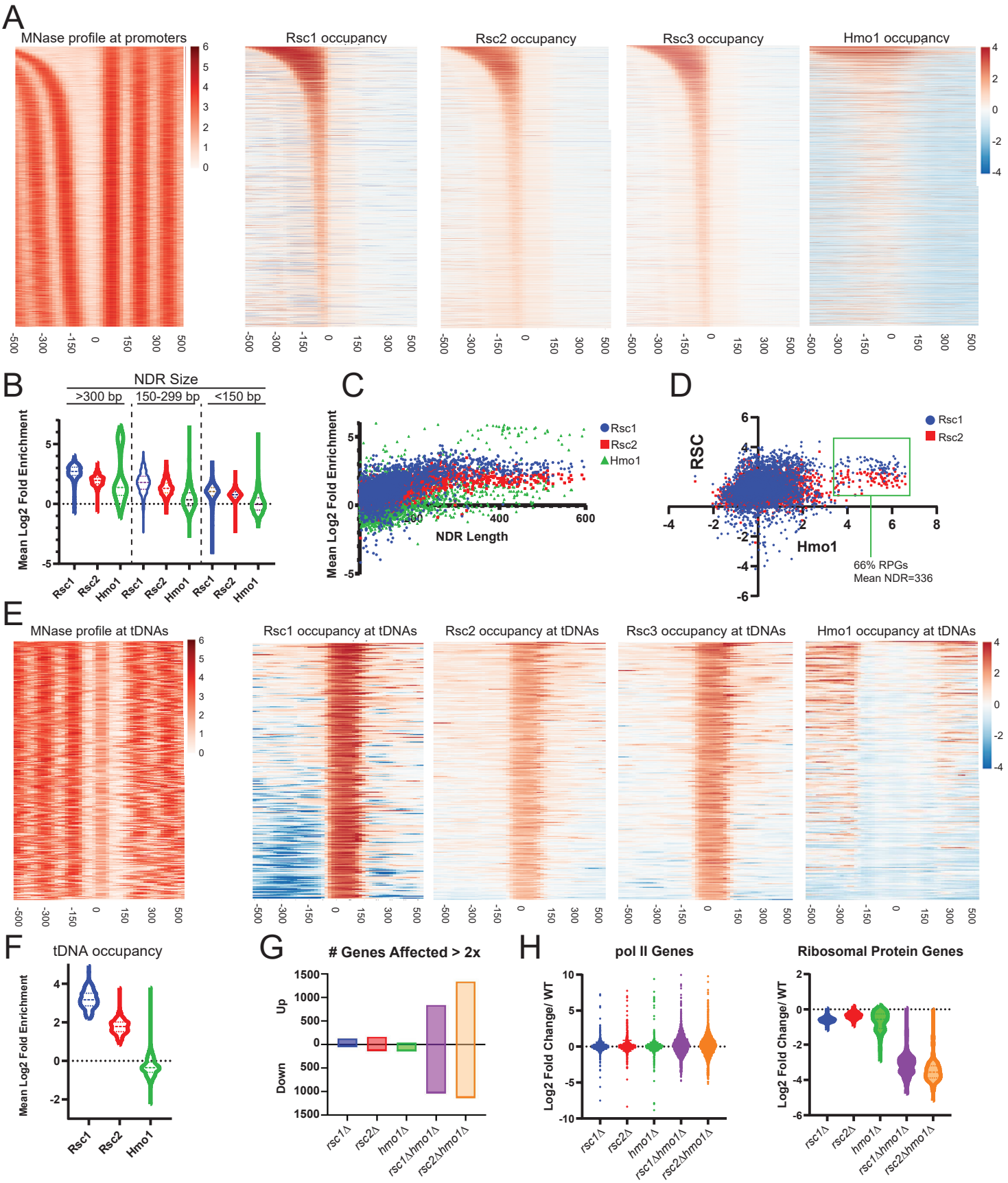

Figure 5. Rsc1 and Rsc2 occupy promoters with wide NDRS, with preferential occupancy of RSC1 at tDNAs. (A) Heat maps showing enrichment of nucleosomes, Rsc1, Rsc2, Rsc3, and Hmo1 at promoters, sorted by NDR length. (B) Violin plot of Rsc1, Rsc2, and Hmo1 occupancy at promoters at three categories of NDR length. (C) Plot of Rsc1, Rsc2, and Hmo1 occupancy compared to NDR length. (D) Plot of Rsc1 and Rsc2 enrichment by Hmo1 occupancy. (E) Heat maps showing enrichment of nucleosomes, Rsc1, Rsc2, Rsc3, and Hmo1 at all tDNAs (tRNA encoding genes). (F) Violin plot of Rsc1, Rsc2, and Hmo1 mean log2 fold enrichment at tDNAs. (G) Number of genes affected by *rsc* and *hmo1* deletions. For each mutation the number of genes up or downregulated two fold or more compared to WT, *rsc1*Δ (↑129↓45), *rsc2*Δ (↑160↓129), *hmo1*Δ (↑44↓132), *rsc1*Δ*hmo1*Δ (↑838↓1028), *rsc2*Δ*hmo1*Δ (↑1336↓1131). (H) Gene Expression changes. Violin plots of RNA expression for each mutation at all pol II genes (6145 genes) and at ribosomal protein genes (132 genes) as compared to WT expression. ChIPSeq and RNASeq data shown represents averages of two and three biological replicates, respectively.

Figure 5 - figure supplement 1. Gene expression changes in *rsc1*Δ, *rsc2*Δ, and *hmo1*Δ mutants.

Figure 5 - figure supplement 2. Gene expression changes in *rsc1*Δ, *rsc2*Δ, and *rsc30*Δ mutants.

Figure 5 - figure supplement 3. Appearance of *RSC1/RSC2*, *RSC3/RSC30*, and *HMO1* in yeast evolution.

Figure 5 - Source Data 1-3.

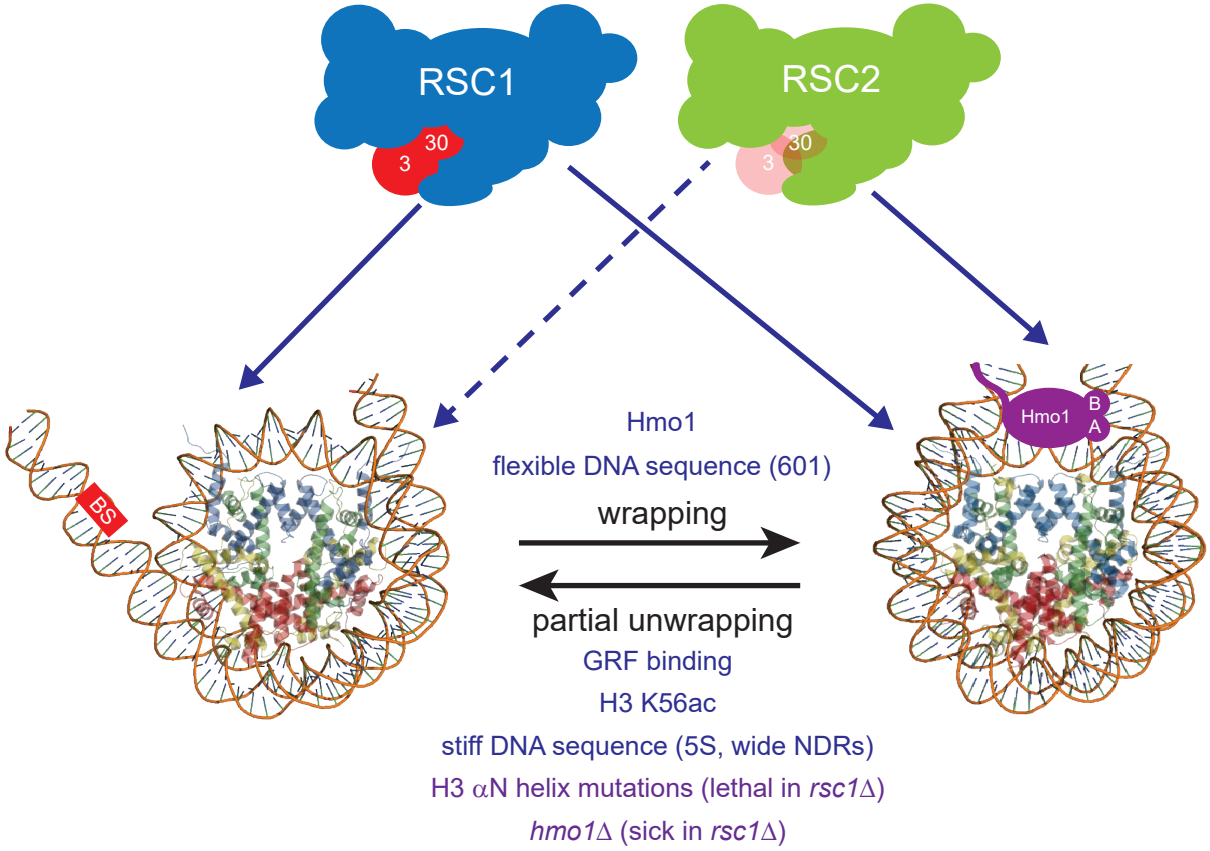

Figure 6. Model for RSC1 and RSC2 action on wrapped versus partially-unwrapped nucleosomes. Here, flexible/positioning DNA sequences and the protein Hmo1 promote wrapping (Anderson et al. 2002, Iyer 2012, Panday and Grove 2017). In contrast, partial unwrapping can be facilitated by 'stiff' (AT-rich) DNA sequences, acetylation (e.g. H3 K56ac), the binding of general regulatory transcription factors (not shown) to entry/exit DNA, or by mutation of residues within/near the H3 αN helix (which normally binds entry/exit DNA) (Segal and Widom 2009, Neumann et al. 2009, Knight et al. 2014, Ferreira et al. 2007). Whereas fully-wrapped nucleosomes are remodeled well by RSC1 or RSC2 complexes, partially-unwrapped nucleosomes are better managed and remodeled by RSC1 complexes.